Accepted Manuscript

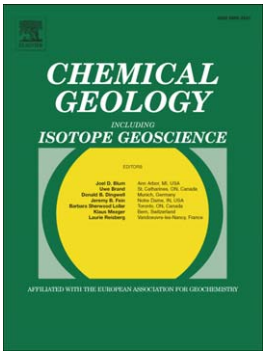

Petrogenesis of rift-related tephrites, phonolites and trachytes (Central European Volcanic Province, Rhön, FRG): Constraints from Sr, Nd, Pb and O isotopes

S. Jung, K. Mezger, F. Hauff, A. Pack, S. Hoernes

PII: S0009-2541(13)00292-1
DOI: doi: 10.1016/j.chemgeo.2013.06.026
Reference: CHEMGE 16936

To appear in: *Chemical Geology*

Received date: 14 December 2011
Revised date: 28 June 2013
Accepted date: 28 June 2013

Please cite this article as: Jung, S., Mezger, K., Hauff, F., Pack, A., Hoernes, S., Petrogenesis of rift-related tephrites, phonolites and trachytes (Central European Volcanic Province, Rhön, FRG): Constraints from Sr, Nd, Pb and O isotopes, *Chemical Geology* (2013), doi: 10.1016/j.chemgeo.2013.06.026

Petrogenesis of rift-related tephrites, phonolites and trachytes (Central European Volcanic Province, Rhön, FRG): constraints from Sr, Nd, Pb and O isotopes

Jung, S.[1*]; Mezger, K.[2], Hauff, F.[3], Pack, A. [4], Hoernes, S.[5]

[1] Universität Hamburg
Dept. Geowissenschaften
Mineralogisch-Petrographisches Institut
20146 Hamburg, Germany
e-mail: stefan.jung@uni-hamburg.de

[2] Institut für Geologie
Universität Bern
Baltzerstrasse 1+3
CH-3012 Bern
Switzerland

[3] IFM-GEOMAR
Research Division 4: Dynamics of the Ocean Floor
Wischhofstrasse 1-3
24148 Kiel, Germany

[4] Georg-August Universität Göttingen
Geowissenschaftliches Zentrum
Abt. Isotopengeologie
Goldschmidtstr. 1
37073 Göttingen; Germany

[5] Mineralogisch-Petrologisches Institut der Universität Bonn
Poppelsdorfer Schloß
53115 Bonn, Germany

Abstract

The volcanic rocks of the Rhön area (Central European Volcanic Province, Germany) belong to a moderately alkali basaltic suite that is associated with minor tephriphonolites, phonotephrites, tephrites, phonolites and trachytes. Based on isotope sytematics ($^{87}Sr/^{86}Sr$: 0.7033-0.7042; $^{143}Nd/^{144}Nd$: 0.51279-0.51287; $^{206}Pb/^{204}Pb$: 19.1-19.5), the inferred parental magmas formed by variable degrees of partial melting of a common asthenospheric mantle source (EAR: European Asthenospheric Reservoir of Cebria and Wilson, 1995). Tephrites, tephriphonolites, phonotephrites, phonolites and trachytes show depletions and enrichments in some trace elements (Sr, Ba, Nb, Zr, Y) indicating that they were generated by broadly similar differentiation processes that were dominated by fractionation of olivine, clinopyroxene, amphibole, apatite and titaniferous magnetite ± plagioclase ± alkalifeldspar. The fractionated samples seem to have evolved by two distinct processes. One is characterized by pure fractional crystallization indicated by increasing Nb (and other incompatible trace element) concentrations at virtually constant $^{143}Nd/^{144}Nd$ ~ 0.51280 and $^{87}Sr/^{86}Sr$ ~ 0.7035. The other process involved an assimilation-fractional crystallization process (AFC) where moderate assimilation to crystallization rates produced evolved magmas characterized by higher Nb concentrations at slightly lower $^{143}Nd/^{144}Nd$ down to 0.51275. Literature data for some of the evolved rocks show more variable $^{87}Sr/^{86}Sr$ ranging from 0.7037-0.7089 at constant $^{143}Nd/^{144}Nd$ ~ 0.51280. These features may result from assimilation of upper crustal rocks by highly differentiated low-Sr (< 100 ppm Sr) lavas. However, based on the displacement of the differentiated rocks from this study towards lower $^{143}Nd/^{144}Nd$ ratios and modeled AFC processes in $^{143}Nd/^{144}Nd$ vs. $^{87}Sr/^{86}Sr$ and $^{207}Pb/^{204}Pb$ vs. $^{143}Nd/^{144}Nd$ space assimilation of lower crustal rocks seems more likely. The view that assimilation of lower crustal rocks played a role is confirmed by high-precision double-spike Pb isotope data that reveal higher $^{207}Pb/^{204}Pb$ ratios (15.62-15.63) in the differentiated rocks than in the primitive basanites (15.58-15.61). This is compatible with incorporation of radiogenic Pb from lower crustal xenoliths ($^{207}Pb/^{204}Pb$: 15.63-15.69) into the melt. However, $^{206}Pb/^{204}Pb$ ratios are similar for the differentiated rocks (19.13-19.35) and the primitive basanites (19.12-19.55) implying that assimilation involved an ancient crustal end member with a higher U/Pb ratio than the mantle source of the basanites. In addition, alteration-corrected $\delta^{18}O$ values of the differentiated rocks range from c. 5 to 7 ‰ which is the same range as observed in the

primitive alkaline rocks. This study confirms previous interpretations that highlighted the role of AFC processes in the evolution of alkaline volcanic rocks in the Rhön area of the Central European Volcanic Province.

Index terms: Igneous petrology, geochemical modeling, radiogenic isotope geochemistry, stable isotope geochemistry, intraplate processes

1. Introduction

Geochemical studies of continental alkaline suites have shown that a particular suite of alkaline rocks commonly evolves along either a strongly silica-undersaturated basanite to phonolite lineage or a less silica-undersaturated alkali basalt to trachyte lineage (e.g., Wilson et al., 1995; Panter et al., 1997). Petrogenetic studies of closely associated silica-undersaturated and silica-saturated rock suites usually invoke complex open system processes to explain their origin from a common parent (Freundt and Schmincke, 1995) and specifically, the assimilation of crust by mantle-derived silica-undersaturated melts to produce oversaturated alkaline magmas (e.g. Foland et al., 1993; Macdonald et al., 1995). Although Foland et al. (1993) favoured a process in which the oversaturated magmas develop from undersaturated felsic parent magmas by AFC processes, they acknowledged that the transition to oversaturation could occur much earlier in the differentiation sequence, with different magmatic lineages bifurcating from a common undersaturated alkaline mafic parent magma. In this study, we use new major and trace element geochemical data, combined with Sr-Nd-Pb-O isotope data, to investigate the processes which led to the contrasting compositions of coexisting highly differentiated alkaline (weakly silica-oversaturated and silica-undersaturated) magma series from the Tertiary Rhön area (Germany). Jung and Hoernes (2000) and Jung et al. (2005) have previously demonstrated that crustal contamination was important in the evolution of the mafic rocks. New isotope data in conjunction with major and trace element and rare earth element (REE) data for the most extreme differentiated rocks (trachytes, phonolites) provide additional constraints on the nature of the likely AFC process that affected the phonolites and trachytes.

2. Geological setting

The Rhön area (Hessia, Bavaria, Thuringia; Germany) extends over ca. 1500 km^2 and lies within the Central European Volcanic Province. In Germany, this province includes (from west to east) the Eifel, the Westerwald, the Vogelsberg, the Hessian Depression, the Rhön area, the Heldburger dyke swarm, and the Oberpfalz area (Fig. 1A). The eruptive centers of these volcanic provinces are aligned perpendicularly to the main NNE-SSW trending rift system of the Upper Rhine valley. This geometry may be interpreted as the result of alpine tectonism further south (Ziegler, 1992). In Germany and elsewhere in Central Europe, Tertiary basin development provides evidence for continental rifting although the huge masses of basaltic rocks in the Vogelsberg area (approximately 500 km^3) and the Cantal (Massif Central, France) cannot be attributed to continental extension alone. The rift segmentation is usually attributed to some minor plume activity because most Tertiary rift faults cross-cut older (Variscan) structures. However, basement uplift is not coeval with the rift development, starting 20-40 Ma after the beginning of rifting (Ziegler, 1992). Whereas some of the Cenozoic volcanism is located mainly on Hercynian fault bounded blocks (e.g. Eifel, Westerwald, Heldburg), the Tertiary volcanic activity in the Rhön area, the Hessian Depression and the Vogelsberg area is restricted to graben-like structures that transect these Hercynian fault bounded blocks. Some of these rift structures (e.g. Rhön area, Hessian Depression) are not associated with basement uplift.

The Rhön area (Fig. 1B) lies at the south-eastern margin of the Hessian Depression which can be interpreted as the northern extension of the Rhine valley. Geophysical data indicate that the Cenozoic rifts are associated with a marked uplift of the Moho discontinuity in which the maximum crustal thinning coincides with the trace of the northern Rhine graben (Ziegler, 1990). Crustal thickness is estimated to be less than 30 km (Prodehl et al., 1992). Babuska and Plomerová (1992) estimated a lithosphere thickness of 100-140 km prior to the Cenozoic rifting and suggested a present-day depth of less than 60 km for the asthenosphere/lithosphere boundary beneath the Rhenish Massif (Fig.1C). Principally, the region has a number of features similar to continental rift zones, being essentially an extensional region with variable but high heat flow and generally thin crust and lithospheric mantle.

Volcanism throughout the entire province is restricted mainly to the Cenozoic; in the Rhön area volcanism started during the Late Oligocene, continued into the Middle Miocene (26-11 Ma; Lippold, 1982) and culminated between 22 and 18 Ma with the voluminous eruption of mainly alkali basalts followed by phonolites, tephrites, basanites and nephelinites, some of them hornblende-bearing. The majority of the phonolites and trachytes and some less strongly differentiated rocks (i.e., tephrites) occur in the western sector of the Rhön area. Wedepohl et al. (1994) proposed a large crustal magma reservoir as the source of these highly differentiated rocks because of their small range in age and composition. However, the large distance (ca. 30 km) between some of the phonolite occurrences renders this suggestion unlikely. In the western sector of the Rhön phonolites are abundant but the predominant basalt types are amphibole-bearing basanites. The latter may represent the parental basalt prior to differentiation. The Hercynian basement into which the alkaline volcanic rocks intruded consists mainly of greenschist to amphibolite-facies metapelites, metabasites and orthogneisses of the Mid German Crystalline Rise and is overlain by Mesozoic and Cenozoic sandstones, carbonates and clays. Sample locations are given in Table 1.

3. Analytical techniques

Whole rock samples were prepared by crushing in an agate shatterbox in order to obtain ca. 250 g of the macroscopically freshest material. Fused lithium-tetraborate glass beads prepared from powder aliquots were analyzed for major and trace elements using standard XRF techniques at the Mineralogisch-Petrographisches Institut, Universität Hamburg. Chromium, Ni, Co and Pb were determined by flameless atomic absorption spectrometry using the graphite furnace technique and Rb was determined by flame atomic absorption spectrometry at the Mineralogisches Institut der Universität Marburg. The precision of each technique is better than 5-10% for all trace elements and the agreement between XRF and atomic absorption spectrometry is generally better than 5%. REE were analyzed by inductively coupled plasma emission spectrometry following separation of the matrix elements by ion exchange (Heinrichs and Herrmann, 1990). Loss on ignition (LOI) was determined gravimetrically at 1050^{o}C (Lechler and Desilets, 1987).

Some Sr and Nd isotope analyses (samples 9, 14, 16, 17) were carried out at the Max-Planck-Institut für Chemie, Mainz using thermal ionization mass spectrometry (TIMS) on a Finnigan MAT

261 multiple sample, multicollector mass spectrometer operating in static mode. The Sr and Nd isotope composition of some samples (samples 3, 8, 13, 15, 26) was measured at the Institut für Mineralogie, Universität Münster on a Finnigan TRITON multicollector mass spectrometer. Whole rock chips were leached in 6N HCl for at least 6 hours. The leachate was decanted, saved and measured separately. The residues were thoroughly rinsed three times with Millipore® water. For the Rb-Sr and Sm-Nd isotope analyses, the samples were spiked with a $^{149}Sm/^{150}Nd$ and a $^{85}Rb/^{84}Sr$ tracer after leaching. In Mainz, Sr and REE were separated using standard cation exchange columns with a DOWEX® AG 50 W-X 12 resin and 2.5N HCl for Sr and 6N HCl for the REE. Nd was separated from the other REE using HDEHP coated Teflon® columns and 0.12 N HCl. In Münster, Sr and REE were extracted as above but Nd was collected using 0.17 N HCl from similar HDEHP coated Teflon® columns. Neodymium isotopes were normalized to $^{146}Nd/^{144}Nd = 0.7219$ at both institutes. Repeated measurements of the La Jolla Nd standard gave $^{143}Nd/^{144}Nd = 0.511848 \pm 0.000021$ (2 σ; n = 28) for Mainz and 0.511863 ± 0.000006 (2 σ; n = 33) for Münster. Strontium fractionation was corrected to $^{86}Sr/^{88}Sr = 0.1194$. The value of the Sr standard (NBS 987) at the Max-Planck-Institut in Mainz is $^{87}Sr/^{86}Sr = 0.710224 \pm 0.000024$ (2 σ; n = 14) and 0.710203 ± 0.000023 (2 σ; n = 64) at the Institut für Mineralogie in Münster. In Mainz and Münster, total blanks for Sr and Nd were below 300 ppb and 100 ppb, respectively. A detailed description of the Pb (Double Spike (DS)) isotope analyses performed at IFM-GEOMAR (Kiel, Germany) is found in Hoernle et al. (2011). Leached rock chips (2N HCl at 70°C for 1 hour and triple rinsed with ultrapure water thereafter) were dissolved in a 1:5 mixture of concentrated ultra pure HNO_3 and HF at 150°C, followed by standard chromatography procedures. Pb isotope ratios were determined on a Finnigan MAT262 TIMS using the silica gel technique. DS corrected NBS 981 values (N=87; 2009-2011) with corresponding 2 sigma external uncertainties are $^{206}Pb/^{204}Pb = 16.9418 \pm 0.0025$, $^{207}Pb/^{204}Pb = 15.4998 \pm 0.0024$, $^{208}Pb/^{204}Pb = 36.7252 \pm 0.0062$, $^{207}Pb/^{206}Pb = 0.91488 \pm 0.00004$ and $^{208}Pb/^{206}Pb = 2.16773 \pm 0.00009$. Typical total chemistry blanks range from 10-30 pg Pb.

Oxygen isotopes for samples 9, 14, 16, 17 were analyzed at the University of Bonn on 8-10 mg aliquots of powdered whole-rock samples, using purified F_2 gas for O_2 extraction, followed by conversion to CO_2 (Clayton and Mayeda, 1963). $^{18}O/^{16}O$ measurements were made on a SIRA-9 triple-collector mass spectrometer by VG-Isogas. Analytical uncertainties are < 0.2‰. Other samples (3, 8, 13, 5, 26) were analyzed at the Universität Göttingen. Here, O-isotope analyses were

conducted by infrared (IR) laser fluorination in combination with gas chromatography isotope ratio monitoring gas mass spectrometry (GC-irmMS) (Jones et al., 1999; Sharp, 1990). The gas extraction technique is described in Pack et al. (2007). In brief, 1.0 – 1.3 mg of sample material was loaded along with MORB glass and NBS-28 quartz into a 18-pit nickel sample holder. After evacuation overnight and pre-fluorination, samples were reacted in a ~20 mbar atmosphere of purified F_2 gas (Asprey, 1976) by means of heating with a SYNRAD 50 W CO_2-laser. Liberated O_2 was cleaned of excess F_2 by reacting with NaCl (110°C). In contrast to Pack et al. (2007), who conducted analyses using the dual inlet system of a Finigan DELTA+ gas mass spectrometer, analyses were conducted in continuous flow mode. A fraction of purified sample O_2 was expanded into a stainless steel capillary and transported with He carrier gas through a second trap, where O_2 was again cryofocused at –196°C on a molecular sieve. Sample O_2 was then released at 100°C back into the He carrier gas stream and transported through a 5 Å molecular sieve GC column of a Thermo Gasbench-II. Sample O_2 was injected via an open split valve of the GasBench-II into the source of a THERMO MAT 253 gas mass spectrometer. The signals of $^{16}O^{16}O$ and $^{18}O^{16}O$ were simultaneously monitored on Faraday cups. Sample peaks (m/z = 32) had an amplitude of 20 – 30 V and a full width at half maximum of ~50 s. Reference O_2 was injected before the sample through a second open split valve of the GasBench-II. The external error of a single analysis was ±0.2‰.

4. Mineralogy of lavas

Most differentiated lavas from the Rhön are porphyritic, with ~ 20% phenocrysts in the phonotephrites and tephriphonolites, ~ 25% in the trachytes and ~ 15% in the phonolites. It is therefore probable that some of the scatter in major element variation diagrams arises from crystal accumulation. Plagioclase is a common groundmass phase in the tephriphonolites and phonotephrites. Kaersutitic amphibole is a common phenocryst phase in the intermediate magmas (phonotephrites and tephriphonolites), and occurs with calcic plagioclase, clinopyroxene, magnetite and apatite. Trachytes are dominated by feldspars, some of which have plagioclase cores and orthoclase rims. They contain also green salitic clinopyroxene. In some trachytes, biotite occurs as a phenocryst phase, together with zircon and apatite. Phonolites are characterized by a fine-grained

groundmass of K-feldspar and sodic plagioclase, pale green clinopyroxene and opaque phases. Phenocrysts include orthoclase, green sodic clinopyroxene, amphibole, biotite, apatite and zircon.

5. Summary of compositional features of the parental alkali basalts

The basanites and nephelinites that are parental to the more differentiated rocks treated in this contribution have been the subject of previous studies (Jung and Hoernes, 2000; Jung et al., 2005). Additional data can be found in Freerck-Parpatt (1990), Ehrenberg et al. (1994), Wedepohl et al. (1994), Wedepohl and Baumann (1999). Most nephelinites and basanites are primitive volcanic rocks whereas others show decreasing Cr, Ni, MgO and TiO_2 contents and CaO/Al_2O_3 ratios but increasing Al_2O_3 and incompatible elements (Sr, Zr, Nb, Y, Ce) with increasing SiO_2 indicating fractionation of mainly olivine, clinopyroxene and amphibole. Nephelinites are products of variable degrees of melting as is shown by their decreasing Al_2O_3 and incompatible element content but increasing CaO/TiO_2 ratio with increasing SiO_2. Some chemical features of the primitive members, i.e. high and decreasing CaO/Al_2O_3 ratios and decreasing La but increasing Yb abundances in the sequence nephelinite-basanite-hornblende basalt can be explained by different degrees of melting of a garnet-bearing source in which garnet is progressively eliminated during melting. Negative anomalies of Rb and K in primitive mantle-normalized diagrams and Rb/K vs. K covariations suggest that amphibole was the major OH-bearing mineral phase.

The $^{87}Sr/^{86}Sr$ and $^{143}Nd/^{144}Nd$ ratios of nephelinites and basanites have a restricted range from 0.70325 to 0.70396 and from 0.51279 to 0.51287, respectively. Hornblende-basalts have a larger spread in $^{87}Sr/^{86}Sr$ ratios but a similar spread in $^{143}Nd/^{144}Nd$ ratios which vary between 0.70339 and 0.70420 and 0.51279 and 0.51284, respectively. Strontium isotope compositions of the hornblende basalts are positively correlated with SiO_2 indicating that they interacted with crustal rocks during fractionation. The range of alteration-corrected $\delta^{18}O$ values is between 5.2 and 7.4 ‰. The negative correlation of $\delta^{18}O$ values with Nd isotope compositions suggests that the higher $\delta^{18}O$ values are the result of crustal contamination. However, pristine values of 5.2 and 5.8 ‰ indicate variable mantle endmembers with respect to the O-isotope composition or some crustal contamination of the mafic magmas. Basanites and nephelinites display a large range in their Os isotope composition whereas Pb and Hf isotopes are rather uniform. For the most primitive

basanites, Pb ($^{206}Pb/^{204}Pb$: 19.18 to 19.33; $^{207}Pb/^{204}Pb$: 15.58 to 15.60) as well as Os and Hf isotope compositions ($^{187}Os/^{188}Os$: 0.132-0.150; ε_{Hf}: +6.4 to +8.9) fall within the range of most OIB. Other basanites and nephelinites, although of still primitive composition as suggested by their high MgO, Ni, and Cr contents, have distinctly more radiogenic Os isotope compositions ($^{187}Os/^{188}Os$: 0.160-0.469). Hafnium and Pb isotopes (ε_{Hf}: +6.4 to +8.7; $^{206}Pb/^{204}Pb$: 19.12 to 19.55; $^{207}Pb/^{204}Pb$: 15.59 to 15.61) are broadly similar to the most primitive basanites. The samples with the lowest Os isotopic compositions ($^{187}Os/^{188}Os_{(23\ Ma)}$: 0.132-0.135) have the highest Os concentrations (70-93 ppt). Low Os concentrations (6-43 ppt) of the samples with high $^{187}Os/^{188}Os$ ratios suggest that their melts may have been contaminated by continental crust material thereby overprinting their mantle signatures. Model calculations suggest that the isotope signatures of the samples with very radiogenic Os ratios (initial $^{187}Os/^{188}Os$ up to 0.469) were produced by assimilation of two different lower crustal components; most likely resembling mafic and felsic lower crust.

6. Geochemistry

6.1 Major and trace elements

Major and trace elements are reported in Table 2. Usually, fractionation trends observed for alkali basalts and differentiated rocks diverge from a single alkali basaltic parent with increasing silica content towards a phonolitic or rhyolitic endmember composition (e.g. Wilson et al. 1995, Panter et al. 1997). In the case of the Rhön lavas, the highly evolved rocks straddle the trachyte-phonolite boundary in the total alkalis-SiO_2 diagram (Fig. 2). The ends of the fractionation trends are defined by trachytes and phonolites. With increasing SiO_2 content, TiO_2, MgO, $FeO_{(total)}$ and CaO decrease progressively, whereas Al_2O_3, K_2O and Na_2O generally increase (Fig. 3). The most evolved rocks have the lowest TiO_2 contents. P_2O_5 is higher in the intermediate rocks than in the more mafic end members but decreases progressively towards the phonolites and trachytes (e.g., Panter et al., 1997). Apatite fractionation clearly controls the concentration of P_2O_5, which is low (<0.2 wt%) in phonolites and trachytes but high in tephriphonolites and phonotephrites (0.80-1.80 wt%).

Concentrations of Ni, Cr, Sc and V in the intermediate magmas (tephrites, phonolites, trachytes) are all low and near the detection limit of the XRF analyses. Primitive mantle normalized

trace element variation diagrams for tephrites, phonolites and trachytes are plotted in Fig. 4. Tephrites show broadly similar patterns to the more primitive rocks (Jung and Hoernes, 2000) with distinct troughs at Rb, K, Pb and Ti. Although the data are limited, some of the phonolites and trachytes show distinctive negative anomalies for Sr, Ba, P and Ti. Zirconium shows a positive anomaly.

The REE patterns of tephrites show an increase in LREE and HREE compared to the inferred parental hornblende-bearing basanite or nephelinite (Fig. 5a). Absolute REE abundances in the tephrites are higher than in the primitive basanites and alkali basalts and significant Eu anomalies, positive or negative, are absent. Phonolitic tephrites have similar REE pattern to tephrites but the tephritic phonolite tend to have a REE pattern with MREE depletion (Fig. 5b). Phonolites are slightly MREE-depleted with high La/Yb ratios and small negative Eu anomalies (Fig. 5c). Trachytes are LREE-enriched with little or no depletion in MREE and no negative Eu anomaly.

6.2 Sr, Nd, Pb and O isotopes

Strontium, Nd, Pb and O isotope data are reported in Table 3. Figure 6 shows the variation of initial $^{143}Nd/^{144}Nd$ vs initial $^{87}Sr/^{86}Sr$, the latter obtained on leached residues for differentiated rocks from this study. Data for phonolites from Wedepohl et al. (1994) are also shown. The tephrites, phonotephrites, phonolites, trachytes and the tephriphonolite from this study plot in the ´depleted field´ relative to Bulk Earth in the Sr-Nd isotope diagram similar to other alkaline rocks from central Europe (Wörner et al., 1986; Wilson and Downes, 1991; Wedepohl et al., 1994; Jung and Masberg, 1998; Jung and Hoernes, 2000; Bogaard and Wörner, 2003; Haase et al., 2004; Jung et al., 2006) but slightly below the inferred parental mafic melts. Figure 7 shows the variation of initial $^{143}Nd/^{144}Nd$ vs. MgO for primitive and evolved samples from the Rhön area.

The tephrite, phonolite and trachyte samples analyzed in this study display a narrow range in initial $^{87}Sr/^{86}Sr$ ratios (0.7034-0.7040) and initial $^{143}Nd/^{144}Nd$ ratios (0.51276-0.51280). On the other hand, the data set presented by Wedepohl et al. (1994) shows a large range in initial $^{87}Sr/^{86}Sr$ ratios at almost constant initial $^{143}Nd/^{144}Nd$ ratios.

Initial Pb isotope compositions of the basanites are variable, defining a linear array subparallel to the Northern Hemisphere Reference Line (NHRL). This trend ranges from moderately high $^{206}Pb/^{204}Pb$ ratios (~ 19.0) to slightly more radiogenic values (~ 19.5) similar to other volcanic provinces from the Central European Volcanic Province (Jung et al. 2005; Fig. 8). The differentiated lavas have similar $^{206}Pb/^{204}Pb$ ratios but more radiogenic $^{207}Pb/^{204}Pb$ ratios that extend towards the Pb isotope composition of lower crust as represented by lower crustal xenoliths from the Hercynian Belt (Fig. 8).

Since O-isotopes are very sensitive to weathering, only those values (reported as $\delta^{18}O$ relative to SMOW) obtained from rocks with $H_2O < 1$ % can be considered magmatic (Kyser et al., 1982). Some of the rocks have high LOI values which are positively correlated with the $\delta^{18}O$ value (Fig. 9) suggesting that the $\delta^{18}O$ are not primary and the high values are probably due to low-temperature alteration. We have therefore decided to correct the measured $\delta^{18}O$ values according to the procedure outlined by Ferrara et al. (1985). This procedure gives an extrapolation of the modified values to the H_2O contents of unaltered rocks which are assumed to have 0.5 wt% H_2O in the present case (Fig. 9). Harmon et al. (1987) reviewed the primary H_2O content of alkaline melts which ranges from 0.5 to 2 wt%. They consider an average value of 0.9 wt% H_2O as being primary for alkaline melts; however, the extrapolation to 0.5 wt% will not greatly affect the interpretations. The mafic alkaline rocks show moderately high alteration-corrected O-isotope values that range from 5.1 to 7.3 ‰ that are negatively correlated with $^{143}Nd/^{144}Nd$ istope ratios (Jung and Hoernes, 2000). Most of these values are within the range for continental basalts (6.4±1.1‰; Harmon and Hoefs 1995); however the higher values are a clear indication that crustal contamination also affected the lavas (Jung et al., 2005). Uncorrected oxygen-isotope values for the differentiated rocks are high (7.2-9.2 ‰; Table 3), however, alteration-corrected O-isotope values range from 5.4 to 7.2 ‰ which is essentially the same range as observed in the more primitive alkaline rocks.

7. Discussion

7.1 Fractional crystallisation (FC) processes

Although the major and trace element variations within the alkaline magmas could be

explained by fractional crystallization processes alone, it is clear on the basis of the Sr-Nd-Pb isotope data that crustal contamination must be important in the petrogenesis of the rocks (Figs. 6 and 8). The decrease in MgO, FeO, CaO, Ni and Cr indicates that the fractionating assemblage in the mafic magmas must include both olivine and clinopyroxene. Green sodic clinopyroxene is the most abundant mafic phenocryst in the tephriphonolites and phonotephrites, however, biotite and amphibole are also present in the evolved rocks albeit in small amounts. The most evolved rocks have the lowest TiO_2 contents which are mostly controlled by the fractionation of ilmenite or magnetite. The variation of TiO_2 vs. SiO_2 further indicates that probably some of the alkali basalts with high TiO_2 contents are the parental rocks of the more differentiated members since the least differentiated tephrites have higher TiO_2 abundances than some more primitive basanites. Because TiO_2 behaves compatibly the tephrites cannot be derived from these low-TiO_2 alkali basalts by fractional crystallization processes. The high-TiO_2 members are confined to the hornblende-bearing basanites and nephelinites (e.g., Jung and Hoernes, 2000). Variation of P_2O_5 among the fractionated samples indicates that apatite fractionation clearly controls the concentration of P_2O_5, which is low (<0.2 wt%) in phonolites and trachytes but high in tephriphonolites and phonotephrites (0.80-1.80 wt%). Al_2O_3 concentrations increase with fractionation throughout the series from basanite to phonolite, but they tend to decrease towards the most differentiated phonolites and trachytes. There is unsystematic scatter in Al_2O_3 among the most fractionated samples, i.e., the tephritic phonolite and the two trachytes and two phonolites. Within this group one trachyte and one phonolite have low Al_2O_3 but the remaining three samples (one phonolite, one trachyte and the tephritic phonolite) have high Al_2O_3.

Low Ni, Cr, Sc and V concentrations are compatible with a fractionating assemblage of olivine, clinopyroxene, amphibole and magnetite from the inferred parental hornblende-bearing basanites and nephelinites. The tephritic phonolite and the two trachytes have high Sr (631-1914 ppm) and high Ba (1370-2131 ppm) but the two phonolites have low Sr (94-247 ppm) and low Ba (237-366 ppm) concentrations. The two phonolites and the two trachytes have similar moderately negative Eu anomalies ($Eu/Eu^* \approx 0.68$-0.72) whereas the tephritic phonolite has no Eu anomaly ($Eu/Eu^* \approx 0.97$). In addition, the tephritic phonolite and all the phonolites and one trachyte show a significant depletion in MREE which is shown by higher total REE abundances but similar MREE abundances relative to the moderately fractionated tephrites. Amphibole may be the fractionating

phase that generates the pronounced MREE depletion in the more evolved magmas (e.g. Wörner and Schmincke, 1984; Wilson et al., 1995). In conclusion, feldspar fractionation may have exerted the major control on the abundances of Ba, Sr and Eu in the most differentiated samples; the concomitant fractionation of amphibole and green sodic clinopyroxene had a competing effect on the Al_2O_3 systematics. Finally, the Rb, Ba and K troughs in primitive mantle-normalized element diagrams are probably inherited features from the mafic parent rocks but the distinctive negative anomalies for Sr, Ba, P and Ti among the phonolites and trachytes are consistent with fractionation of plagioclase, K-feldspar, apatite and Ti-magnetite.

7.2 Assimilation Fractional Crystallisation (AFC) processes

Isotope data presented earlier (Wedepohl et al., 1994) clearly indicate the importance of combined assimilation and fractional crystallization (AFC) processes in the petrogenesis of differentiated volcanic rocks from the Central European Volcanic Province. Based on the apparent negative correlation between Nd and Sr isotopes, Wedepohl et al. (1994) suggested that the crustal contaminant must be characterized by radiogenic Sr and unradiogenic Nd. In this model, crustal contamination is probably caused by partial melting of the wall rocks of the magma chamber producing granitic (or tonalitic) partial melts depending on the felsic (or mafic) composition of the wall rocks, respectively. The lower crust beneath the Central European Volcanic Province in Germany is mainly composed of mafic and felsic granulites in which mafic granulites, interpreted as basaltic cumulates, predominate over felsic granulites (Mengel, 1990; Mengel et al., 1991; Sachs and Hansteen, 2000). Comprehensive isotope data are only available for lower crustal xenoliths from the Eifel area (Stosch & Lugmair, 1984; Stosch et al., 1986, 1992; Loock et al., 1990; Rudnick & Goldstein, 1990). These granulites have Sr-Nd isotope compositions that extend from Bulk Earth values towards more unradiogenic $^{143}Nd/^{144}Nd$ but more radiogenic $^{87}Sr/^{86}Sr$ isotope compositions (Liew and Hofmann, 1988).

To model the Nd-Sr isotope variation quantitatively, several parameters must be known including the Sr and Nd contents and isotopic compositions of the parent magma, the bulk distribution coefficients of both Sr and Nd (D^{Sr} and D^{Nd}), the ratio of the mass assimilated to the mass of material fractionated (r) and the isotopic composition of the assimilated material (DePaolo,

1981). Taylor (1980) has estimated that the ratio (r) between the mass of assimilated material and the mass of crystals in an upper crustal basaltic magma chamber with an initial wall rock temperature of ~150 ^{o}C is about 0.3. On the other hand, DePaolo (1981) assumes that this ratio approaches 1 in magma chambers of the lower crust with an initial wall rock temperature of ~1000 ^{o}C. Clearly, clinopyroxene, plagioclase and olivine (and amphibole in the present case) will control the magnitude of the respective bulk distribution coefficients, which will commonly range between 0.2 and 0.5 for Nd and between 0.2.and 1 for Sr.

For the samples analysed in this study, initial $^{143}Nd/^{144}Nd$ ratios are slightly less radiogenic (from ~0.51280 to ~0.51276) than the basalts (Fig. 6) and initial $^{87}Sr/^{86}Sr$ ratios range from ~0.7034 to ~0.7040. This may indicate a contaminant characterized by a relatively low time-integrated Rb/Sr signature. The decrease in radiogenic Nd broadly correlates with sample differentiation and decreasing MgO from basanite to trachyte and phonolite (Fig. 7), as it would be expected during AFC processes. We have modeled the Sr-Nd isotope variation (Fig. 6) with the following parameters for the contaminant based on the granulite sample S 1 from Stosch and Lugmair (1984): $^{87}Sr/^{86}Sr$: 0.704922, 691 ppm Sr, D^{Sr}: 0.5, $^{143}Nd/^{144}Nd$: 0.512608, 43 ppm Nd, D^{Nd}: 0.5. Note that the parameters are fundamentally different to those used by Wedepohl et al. (1994). In addition, the most important change in the parameters is the value of r which was set at 0.4 to allow for moderately high rates of assimilation relative to fractional crystallization which results in a steeper AFC curve. From Fig. 6, it is apparent that the differentiated rocks have undergone assimilation of c. 40%. For the phonolites from the Rhön, Wedepohl et al. (1994) observed an unusual style of contamination that produces high $^{87}Sr/^{86}Sr$ ratios up to 0.7090. These phonolites have low Sr abundances (average 59 ppm with Eu/Eu*: 0.65) suggesting the involvement of plagioclase during fractionation and consequently upper crustal contamination was inferred. A similar case with different $^{87}Sr/^{86}Sr$ ratios was presented by Wörner et al. (1985) for the Laacher See Tephra Sequence of the East Eifel and was interpreted to represent shallow assimilation late in the magmatic history. Here, the evolution from high-Sr samples with 300 ppm Sr towards low-Sr samples with 4 ppm Sr was also accompanied by an increase in $^{87}Sr/^{86}Sr$ from 0.705 to 0.711. The samples treated in our study show higher Sr (94-1914 ppm; Eu/Eu*: 0.72-0.68) and unradiogenic $^{87}Sr/^{86}Sr$ ratios. It is obvious that the observed distinct style of contamination is due to differences in the Sr content corresponding to distinct degrees of differentiation involving distinct amounts of

plagioclase. This may indicate contamination at different crustal levels.

The isotope variations imply that the trachytes and phonolites have undergone some assimilation of lower crustal rocks during fractional crystallization (AFC processes). Some incompatible trace element concentrations predicted by fractional crystallization curves at c. 20-30% magma remaining (Fig. 10) are similar to measured values of phonolitic and trachytic compositions. Hypothetical lower crustal rocks are inferred to be less radiogenic in $^{143}Nd/^{144}Nd$ than the alkali basalts and the differentiated rocks. Panter et al. (1997) have suggested that assimilation of lower crustal rocks by highly differentiated magmas may occur at low mass assimilation to mass crystallization rates and low F values producing melts with low $^{143}Nd/^{144}Nd$ ratios and high abundances of incompatible elements. Using Nb as an example, an AFC evolutionary path cannot extend below the Nb content of the inferred initial mafic magma (~ 74 ppm), assuming that D^{Nb} is < 1. Thus, assimilation by differentiated magmas will produce compositions that evolve away from the field of the parental magmas towards lower $^{143}Nd/^{144}Nd$ and higher Nb concentrations (Fig. 10). Neodymium behaves incompatibly during differentiation and its abundance in basaltic melts is roughly similar to that of the contaminant. Hence, in AFC model calculations, basaltic magmas are displaced towards the Nd isotopic composition of the lower crustal wallrock much more efficiently than are contaminated, highly evolved magmas. On a graph of $^{143}Nd/^{144}Nd$ versus a highly incompatible element (Fig. 10), AFC curves will be steeper for less evolved magmas and flatten out for more evolved compositions. This effect is accentuated with changes in the rate of assimilation to crystal fractionation (*r*). F values (where F=fraction of melt remaining) in our model extend to 0.5 indicating a moderate degree of fractionation. In Fig. 10, the calculated AFC path shows an apparent small misfit between the computed and measured values. For the calculation of the AFC curve we have used values from the same xenolith (sample S 1 from Stosch and Lugmair, 1984) that was used to model the AFC path in Sr-Nd-Pb space. Small deviations of computed to measured values can be expected since it is very unlikely that one single xenolith is representative in term of its Sr-Nd-Pb isotope composition and Sr, Nd, Pb and incompatible trace element concentrations. High *r*-values (> 0.7) are suggested for basaltic AFC whereas low r paths (< 0.5) fit more evolved compositions (i.e. Panter et al., 1997). This may be explained by differentiation of basaltic magmas at deep levels in the crust, where high ambient wallrock temperatures and hot basic magmas facilitate higher rates of assimilation (Davidson and

Wilson, 1989; Shaw et al., 1993; Reiners et al., 1995).

The Pb isotope data of the parental basanites plot on the Northern Hemisphere Reference Line (NHRL) whereas the Pb isotope compositions of the xenoliths plot above the NHRL in $^{207}Pb/^{204}Pb$ vs. $^{206}Pb/^{204}Pb$ and $^{208}Pb/^{204}Pb$ vs. $^{206}Pb/^{204}Pb$ space (Fig. 8). The differentiated lavas have $^{206}Pb/^{204}Pb$ ratios similar to the basanites but have distinctly more radiogenic $^{207}Pb/^{204}Pb$ ratios suggesting assimilation of an ancient crustal component having a high U/Pb history. Using Pb isotope and concentration data for xenolith sample S 1 ($^{207}Pb/^{204}Pb$: 15.66, 5.1 ppm Pb) from Rudnick and Goldstein (1990), AFC modelling produces a fair match of the sample data with the modelled AFC curve (Fig. 11).

It has been shown above that crustal contamination via an AFC process is monitored by decreasing $^{143}Nd/^{144}Nd$ isotope ratios with decreasing MgO (Fig. 7). Similarly, alteration-corrected $\delta^{18}O$ values (Fig. 9) are higher than upper mantle values which may be caused by AFC processes, hydrous alteration or both. Whether or not the correction procedure of Ferrara et al. (1985) can be applied to the samples studied here is debatable. Clearly, hydrous alteration must have played a role but the results from recent studies in the Siebengebirge (Fig. 1) have shown that there is a clear 1:1 correlation of O isotope values obtained on mineral separates with the alteration-corrected $\delta^{18}O$ values of the respective whole rocks (Jung et al. in 2012). This shows that the alteration correction may work in this case; whether it is applicable to other volcanic series needs to be tested.

The complex geochemical variations of the Rhön volcanic rocks are best modeled by magmatic differentiation along two major lineages: (1) fractional crystallization of alkali basalt or probably hornblende-bearing basanite to produce the high Nb-trachytes and phonolites and (2) assimilation of crust by basanite or nephelinite and concurrent crystal fractionation evolving to trachyte with high Nb contents but unradiogenic $^{143}Nd/^{144}Nd$ and radiogenic $^{207}Pb/^{204}Pb$ (Figs. 6, 10 and 11). The ascent of alkali basalts *sensu lato* through the lithosphere was probably arrested at a level where reaction with crust could occur at moderately high assimilation to fractional crystallization rates. Based on isenthalpic AFC calculations, Reiners et al. (1995) determined that high r values can result during early stages of basalt contamination when country rock temperatures are between 400 and 800°C.

8. Summary and conclusion

Previous geochemical and isotopic studies on mafic alkali basalts (nephelinites, basanites) from the Rhön area have shown that most of these represent near-primary asthenosphere- or lower lithosphere derived melts produced by a few percent partial melting of garnet peridotite containing residual amphibole (Jung and Hoernes, 2000). The intermediate to evolved magmas (tephriphonolites, phonotephrites, phonolites, trachytes) of the alkaline suite of the Rhön have distinct major and trace element and isotope characteristics that provide important constraints on their petrogenesis. The differentiated rocks evolved from parental probably hornblende-bearing basanites along a differentiation trend that is controlled by separation of olivine, clinopyroxene, amphibole, ± plagioclase, ± K-feldspar, apatite and magnetite. Depletion of MREE in some samples points to amphibole fractionation whereas depletion of Ba, Sr and Eu is caused by fractionation of feldspars. Previous studies on differentiated alkaline rocks (i.e., Wilson et al., 1995) have shown that such suites may evolve by AFC processes in which assimilation may cease after 55-65% fractional crystallization but further differentiation may occur beyond this point. The alkaline suite from the Rhön follow two isolated paths; one is characterized by AFC and the other path reflects pure fractional crystallization, both from slightly different parental alkali basalts. Model calculations indicate that the Sr and Nd isotope composition of the inferred contaminant had little obvious effect on the Sr and Nd isotope composition of the lavas. On the other hand, the effect for the Pb isotope composition is significant. Therefore, qualitative constraints on the composition of the contaminant require ancient granulite facies lower crustal rocks with low Rb/Sr, low Sm/Nd coupled with moderate Nd concentrations and elevated U/Pb ratios coupled with moderate to high Pb concentrations. In addition, this study places important constraints on distinct contamination scenarios at different levels within the crust. This study shows that deep crustal assimilation is hardly detectable in high-Sr phonolites and trachytes (Sr >> 100 ppm) but may be recognized by subtle variations in Nd, Pb and O isotope compositions. Other studies (e.g. Wedepohl et al., 1994) indicated that low-Sr phonolites (Sr << 100 ppm) are probably more prone to show effects of crustal contamination due to the strong contrast in Sr concentrations and isotope compositions between these phonolites and lower or upper crustal country rocks. On a regional scale, isotope studies on differentiated alkaline rocks from the Central European Volcanic Province have shown that evolved lavas from the Eifel do not show elevated $^{207}Pb/^{204}Pb$ ratios (Jung et al., 2005) whereas

differentiated lavas from the Westerwald (Haase et al., 2004) and the Siebengebirge (Jung et al. 2012; Kolb et al., 2012) have high $^{207}Pb/^{204}Pb$ up to 15.68. Hence, crustal contamination is a common phenomenon in evolved alkaline lavas and substantial variation in lower crustal compositions beneath the different volcanic fields of the Central European Volcanic Province may exist.

Acknowledgements

The senior author appreciates the help and advice of H. Baier (Münster) during a short visit there. Some Sr and Nd isotope measurements were made possible by the Max-Planck-Institut für Chemie in Mainz while S.J. was on leave from the institute and the senior author appreciates the hospitality and support throughout the years. As usually, Iris Bambach (Mainz) produced high-quality figures and her help is highly appreciated. Detailed reviews by G. Wörner and J.M. Cebriá resulted in significant improvements and are highly appreciated and we would like to thank Laurie Reisberg for patient and efficient editorial handling.

References

Adam, J., Green, T. 2006. Trace element partitioning between mica- and amphibole-bearing garnet lherzolite and hydrous basanitic melt: 1. Experimental results and the investigation of controls on partitioning behavior. Contrib. Mineral. Petrol. 152, 1-17.

Adam, J., Green, T.H., Sie, S.H. 1993. Proton microprobe determined partitioning of Rb, Sr, Ba, Y, Zr, Nb and Ta between experimentally produced amphiboles and silicate melts with variable F content. Chem. Geol. 109, 29-49.

Asprey, L. B. 1976. The preparation of very pure F_2 gas. J. Fluor. Chem. 7, 359-361.

Babuska, V., Plomerova, J. 1992. The lithosphere in Central Europe - seismological and petrological aspects. Tectonophysics 207, 101-163.

Bogaard P.J.F., Wörner, G. 2003. Petrogenesis of basanitic to tholeiitic volcanic rocks from the Miocene Vogelsberg, Central Germany. J. Petrol. 44, 569-602.

Boynton, W.V. 1984. Geochemistry of the rare earth elements: meteorite studies. In: Henderson, P. (ed), Rare earth element geochemistry. Elsevier, 63-114.

Cebriá, J. M., Wilson, M. 1995. Cenozoic mafic magmatism in Western/Central Europe: A common asthenospheric reservoir? Terra Nova, Abstracts Supplement, 7, 162.

Davidson, J. P., Wilson, I. R. 1989. Evolution of an alkali basalt–trachyte suite from Jebel Marra volcano, Sudan, through assimilation and fractional crystallization. Earth Planet. Sci. Lett. 95, 141–160.

DePaolo, D.J. 1981. Trace element and isotopic effects of combined wallrock assimilation and fractional crystallization. Earth Planet. Sci. Lett. 53, 189-202.

Engelhardt, H. J. 1990. TUC-Referenzproben in Geochemie und Umweltanalytik. Mitteillungsblatt TU Clausthal 70, 26-28.

Ehrenberg, K.H., Hickethier, H., Rosenberg, F.,Strecker, G., Susic, M., Wenzel, G. 1992. Neue Ergebnisse zum tertiären Vulkanismus der Rhön (Wasserkuppenrhön und Kuppenrhön). Eur. J. Mineral. Beih. 2, 47-102.

Ehrenberg, K. H., Hansen, R., Hickethier, H, Laemmlen, M. 1994. Erläuterungen zur geologischen Karte von Hessen, Blatt 5425 Kleinsassen. Hess. Landesamt Bodenforsch. 385 pp.

Ewart, A. and Griffin, W.L. (1994). Application of Proton-Microprobe Data to Trace-Element Partitioning in Volcanic-Rocks. Chem. Geol. 117, 251-284.

Ferrara, G., Laurenzi, M. A., Taylor, H. P., Toranini, S., Turi, P. 1985. Oxygen and strontium isotope studies of K-rich volcanic rocks from the Alban Hill, Italy. Earth. Planet. Sci. Lett., 75, 13-28.

Freerck-Parpatt, M. 1990. Geochemie Amphibol-führender Nephelinbasanite und Alkaliolivinbasalte aus der Rhön. PhD thesis, Universität Göttingen, 98 pp.

Foland, K. A., Landoll, J. D., Henderson, C. M. B., Jianfeng, C. 1993. Formation of cogenetic quartz and nepheline syenites. Geochim. Cosmochim. Acta 57, 697-704.

Freundt, A., Schmincke, H-U. 1995. Petrogenesis of rhyolite–trachyte–basalt composite ignimbrite P1, Gran Canaria, Canary Islands. J. Geophy. Res. 100, 455–474.

Govindaraju, K. (eds.) (1994) Compilation of working values and sample description for 383 geostandards. Geostandards Newsletters 17, 158 pp.

Haase, K. M., Goldschmidt, B., Garbe-Schönberg, D. 2004. Petrogenesis of Tertiary continental intra-plate lavas from the Westerwald region. J. Petrol. 45, 883-905

Harmon, R.S., Hoefs, J., Wedepohl, K. H. 1987. Stable isotope (O, H, S) relationships in Tertiary basalts and their mantle xenoliths from the Northern Hessian Depression, W.- Germany. Contrib. Mineral. Petrol. 95, 350-369.

Hart, S.R. 1984. A large-scale isotope anomaly in the southern hemisphere mantle. Nature 309, 753-757.

Heinrichs, H., Herrmann, A. G. 1990. Praktikum der analytischen Geochemie. Springer. Berlin-Heidelberg-New York.

Hoernle, K., Hauff, F., Kokfelt, T.F., Haase, K., Garbe-Schönberg, D., Werner, R., 2011. On- and off-axis chemical heterogeneities along the South Atlantic Mid-Ocean-Ridge (5-11°S): Shallow or deep recycling of ocean crust and/or intraplate volcanism? Earth Planet. Sci. Lett.,, 86-97.

Jones, A. M., Iacumin, P., Young, E. D. 1999. High-resolution $\delta^{18}O$ analysis of tooth enamel phosphate by isotope ratio monitoring gas chromatography mass spectrometry and ultraviolet laser fluorination. Chem. Geol. 153, 241-248.

Jung, S., Masberg, P. 1998. Major- and trace element systematics and isotope geochemistry of Cenozoic mafic volcanic rocks from the Vogelsberg (Central Germany) - Constraints on the origin of continental alkaline and tholeiitic basalts and their mantle sources. J. Volc. Geotherm. Res. 86, 151-177.

Jung, S., Hoernes, S. 2000. The major- and trace element and isotope (Sr, Nd, O) geochemistry of Cenozoic alkaline rift-type volcanic rocks from the Rhön area (central Germany): Petrology, mantle source characteristics and implications for asthenosphere-lithosphere interactions. Jour. Volc. Geotherm. Res. 99, 27-53.

Jung, S., Pfänder, J. A., Brügmann, G., Stracke, A. 2005. Sources of primitive alkaline volcanic rocks from the central European Volcanic province (Rhön, Germany) inferred from Hf, Pb and Os isotopes. Contrib. Mineral. Petrol. 150, 546-559.

Jung, C., Jung, S., Hoffer, E., Berndt, J. 2006. Petrogenesis of Tertiary mafic alkaline magmas from the Hocheifel, Germany. J. Petrol. 47, 1637-1671.

Jung, S., Vieten, K., Romer, R.L., Mezger, K., Hoernes, S., Satir, M. 2012. Petrogenesis of Tertiary alkaline magmas in the Siebengebirge, Germany. J. Petrol., 53, 2381-2409.

Kolb, M., Paulick, H., Kirchenbaur, M., Münker, C. 2012. Petrogenesis of mafic to felsic lavas from the Oligocene Siebengebirge Volcanic Field (Germany): Implications for the origin of

intracontinental volcanism in Central Europe J. Petrol., 53, 2349-2379..

Kyser, T.K., O´Neil, J. R., Carmichael, I. S. E. 1982. Genetic relations among basic lavas and ultramafic nodules: evidence from oxygen isotope composition. Contrib. Mineral. Petrol. 81, 88-102.

Lechler, P.J., Desilets, M. O. 1987. A review of the use of loss on ignition as a measurement of total volatiles in whole rock analysis. Chem. Geol. 63, 341-344.

Liew, T.C., Hofmann, A. W. 1988. Precambrian crustal components, plutonic associations, plate environment of the Hercynian Fold Belt of central Europe: indications from a Nd and Sr isotopic study. Contrib. Mineral. Petrol. 98, 129 138

Lippolt, H. J. 1982. K/Ar age determinations and the correlation of Tertiary volcanic activity in Central Europe. Geol. Jb. Hannover D 52, 113-135.

Loock, G., Stosch, H.-G. & Seck, H. A. 1990. Granulite facies lower crustal xenoliths from the Eifel, West Germany: petrological and geochemical aspects. Contrib. Mineral. Petrol. 195, 25-41.

Macdonald, R., Davies, G. R., Upton, B. G. J., Dunkley, P. N., Smith, M., Leat P. T. 1995. Petrogenesis of Silali volcano, Gregory Rift. J. Geol. Soc. London 152, 703–720.

Mahood, G.A., Stimac, J.A. 1990. Trace-element partitioning in pantellerites and trachytes. Geochim. Cosmochim Acta 54, 2257-2276.

Matsui, Y., Onuma, N., Nagasawa, H., Higuchi, H., Banno, S. 1977. Crystal structure control in trace element partition between crystal and magma. Tectonics 100, 315-324.

Mengel, K. 1990. Crustal xenoliths from Tertiary volcanics of the Northern Hessian Depressian. Contrib. Mineral. Petrol. 104, 8-26.

Mengel, K., Sachs, P. M., Stosch, H. G., Wörner, G., Loock G., 1991. Crustal xenoliths from Cenozoic volcanic fields of West Germany: implications for structure and composition of the crust. Tectonophysics. 195, 271–289.

Pack, A., Toulouse, C. Przybilla, R. 2007. Determination of oxygen triple isotope ratios of silicates without cryogenic separation of NF_3 — technique with application to analyses of technical O_2 gas and meteorite classification. Rap. Comm. Mass Spectr. 21, 3721-3728.

Panter, K. S., Kyle, P. R., Smellie J. L. 1997. Petrogenesis of a Phonolite-Trachyte succession at Mount Sidley, Marie Byrd Land, Antartica. J. Petrol.. 38, 1225-1253.

Prodehl, C., Müller, S., Glahn, A., Gutsher, M., Haak, V. 1992. Lithosphere cross-section of the European rift system. In: PA Ziegler (ed), Geodynamics of rifting, Vol. 1. Case histories on rifts: Europe and Asia. Tectonophysics. 208, 113-138.

Reiners, P. W., Nelson, B. K., Ghiorso M. S. 1995. Assimilation of felsic crust by basaltic magma: thermal limits and extents of crustal contamination of mantle-derived magmas. Geology 23, 563–566.

Rudnick, R.L., Gao, S. 2004. Composition of the Continental Crust. In: Treatise on Geochemistry. Holland, H.D. and Turekian, K.K. (Editors), Elsevier, Amsterdam. 3: 1-64.

Rudnick, R., Goldstein, S. L. 1990. The Pb isotopic evolution of lower crustal xenoliths and the evolution of lower crustal Pb. Earth Planet. Sci. Lett. 98, 192-207.

Sachs, P. M., Hansteen, T. H. 2000. Pleistocene underplating and metasomatism of the lower continental crust: a xenolith study. J. Petrol. 41, 331–356.

Sharp, Z. D. 1990. A laser-based microanalytical method for the in situ determination of oxygen isotope ratios of silicates and oxides. Geochim. Cosmochim. Acta. 54, 1353-1357.

Shaw, A., Downes, H., Thirlwall M. F. 1993. The quartz-diorites of Limousin: elemental and isotopic evidence for Devono-Carboniferous subduction in the Hercynian belt of the French Massif. Chem. Geol. 107, 1–18.

Stosch, H.-G., Lugmair, G. W. 1984. Evolution of the lower continental crust: granulite facies xenoliths from the Eifel, West Germany. Nature 311, 368-370.

Stosch, H.-G., Lugmair, G. W. 1986. Trace element and Sr and Nd isotope geochemistry of peridotite xenoliths from the Eifel (West Germany) and their bearing on the evolution of the subcontinental lithosphere. Earth Planet. Sci. Lett. 80, 281-298.

Stosch, H.-G., Lugmair, G. W., Seck, H. A. 1986. Geochemistry of granulite-facies lower crustal xenoliths: implications for the geological history of the lower continental crust below the Eifel, West Germany. In: Dawson, J. B., Carswell, D. A., Hall, J. & Wedepohl, K. H. (eds) The Nature of the Lower Continental Crust. Geological Society, London, Special Publications 24, 309–317.

Stosch, H-G., Schmucker, A., Reys, C. 1992. The nature and geological history of the deep crust under the Eifel, Germany. Terra Nova 4, 53-62.

Sun, S.-S., McDonough, W. F. 1989. Chemical and isotopic systematics of oceanic basalts: implications for mantle composition and processes. in: Saunders, A.D., M. J. Norry (eds). Magmatism in the ocean basins. Geol. Soc. Spec. Publ. 42, 313-345.

Taylor, H. P. 1980. The effects of assimilation of country rocks by magmas on $^{18}0/^{16}0$ and $^{87}Sr/^{86}Sr$ systematics in igneous rocks. Earth Planet. Sci. Lett 47, 243 254

Villemant, B., Jaffrezic, H., Joron, J.L., Treuil, M. 1981. Distribution coefficients of major and trace elements - fractional crystallization in the alkali basalt series of Chaine-Des-Puys (Massif Central, France). Geochim. Cosmochim. Acta 45, 1997-2016.

Wedepohl, K. H., Baumann, A. 1999. Central European Cenocoic plume volcanism with OIB characteristics and indications of a lower mantle source. Contrib. Mineral. Petrol. 136, 225-239.

Wedepohl, K.H., Gohn, E., Hartmann, G. 1994. Cenozoic alkali basaltic magmas of western Germany and their products of differentiation Contrib. Mineral. Petrol. 115, 253-278.

Witt-Eickschen, G., Seck, H. A., Mezger, K., Eggins, S. M. & Altherr, R. 2003. Lithospheric mantle evolution beneath the Eifel (Germany): Constraints from Sr-Nd-Pb isotopes and trace element abundances in spinel peridotite and pyroxenite xenoliths. J. Petrol 44, 1077-1095.

Witt-Eickschen, G., Kaminsky, W., Kramm, U., Harte, B. 1998. The nature of young vein metasomatism in the lithosphere of the West Eifel (Germany): Geochemical and isotopic constraints from composite mantle xenoliths from the Meerfelder Maar. J. Petrol 39, 155-185.

Wilson, M., Downes, H. 1991. Tertiary-Quarternary extension-related alkaline magmatism in Western and Central Europe. J. Petrol., 32, 811-849

Wilson, M., Downes, H. , Cebria, J.-M. 1995. Contrasting fractionation trends in coexisting continental alkaline magma series; Cantal, Massif Central, France. J. Petrol. 36, 1729-1753.

Wörner, G., Schmincke, H.-U. 1984. Mineralogical and chemical zonation of the Laacher See Tephra Sequence (E. Eifel, W. Germany). J. Petrol., 25, 805-835.

Wörner, G., Staudigel, H., Zindler, A. 1985. Isotopic constraints on open system evolution of the Laacher See magma chamber (Eifel, West Germany). Earth Planet. Sci. Lett. 75, 37-49.

Wörner, G., Zindler, A., Staudigel, H. , Schmincke, H. U. 1986. Sr, Nd, and Pb isotope geochemistry of Tertiary and Quarternary alkaline volcanics from West Germany. Earth Planet. Sci. Lett. 79, 107-119

Zack, T., Brumm, R. 1998. Ilmenite/liquid partition coefficients of 26 trace elements determined through ilmenite/clinopyroxene partitioning in garnet pyroxene. In: 7th International Kimberlite Conference. Gurney, J.J., Gurney, J.L., Pascoe, M.D., Richardson, S.H. (Editors), Red Roof Design, Cape Town, 986-988.

Ziegler, P. A. 1990. Geological atlas of Eastern and Central Europe. 2nd edition Shell Int. Pet. Mij. Geol. Soc. Publ. Bath. 238 pp.

Ziegler, P. A. 1992. European Cenozoic rift system. In: Ziegler, P. A. (ed), Geodynamics of rifting, Vol. 1. Case histories on rifts: Europe and Asia. Tectonophysics 208, 91-111.

Figure captions:

Figure 1(A): Distribution of Cenozoic volcanic rocks in Central Europe (slightly modified from Wedepohl et al., 1994). Numbers denote K-Ar ages from Lippolt (1982). (B): Location of the Rhön volcanic province. (C): Contour map of lithosphere thickness in Europe (Wedepohl et al., 1994).

Figure 2: Total Alkali-Silica (TAS) diagram for the alkaline rocks from the Rhön area.

Figure 3: Major oxide and trace element Harker diagrams showing the distribution of the alkaline rocks from the Rhön area.

Figure 4: Primitive mantle-normalized incompatible element patterns of tephrites, phonolites and trachytes. Grey shaded fields denotes trace element abundances of basanites and nephelinites (Jung and Hoernes, 2000 and upublished data). Normalization values from Sun and McDonough (1989).

Figure 5: Chondrite-normalized REE diagram of (a) tephrites, (b) phonolitic tephrites and tephritic phonolite and (c) phonolites and trachytes. Normalization values from Boynton (1984). Grey field denotes REE abundances of basanites and nephelinites (Jung and Hoernes, 2000 and upublished data).

Figure 6: $^{143}Nd/^{144}Nd$ vs. $^{87}Sr/^{86}Sr$ diagram showing data for alkali basalts (Jung and Hoernes,

2000) and phonolites (Wedepohl et al., 1994) from the Rhön area. Also shown is a modelled AFC path with the following parameters for the inferred parental basanite (51 ppm Nd; $^{143}Nd/^{144}Nd$ = 0.512851, 890 ppm Sr; $^{87}Sr/^{86}Sr$: 0.70342; sample 1a from Jung and Hoernes, 2000) and the hypothetical lower crustal rock (42.6 ppm Nd, $^{143}Nd/^{144}Nd$: 0.512608; 691 ppm Sr, $^{87}Sr/^{86}Sr$: 0.704921: sample S 1 from Stosch and Lugmair, 1984). Bulk Kds for Nd and Sr were 0.5, respectively. R (the ratio of mass assimilated to mass fractionated) was set at 0.4 to allow for lower crustal melting at elevated temperatures. Small white circles on the AFC curve represent 10% increments of assimilation. Dark grey area represents Eifel peridotite xenolith data from Witt-Eickschen et al. (1998, 2003) and Stosch and Lugmair (1986). Stippled area represent Sr and Nd isotope data from Tertiary Central European Volcanic Province alkali basalts compiled by Lustrino and Wilson (2007). Light grey field represents Eifel lower crustal xenolith data (Loock et al., 1990; Stosch and Lugmair, 1984).

Figure 7: $^{143}Nd/^{144}Nd$ vs. MgO for tephrites, phonolites and trachytes. Also shown are data for alkali basalts from Jung and Hoernes (2000).

Figure 8: Plot of (a) $^{207}Pb/^{204}Pb$ and (b) $^{208}Pb/^{204}Pb$ versus $^{206}Pb/^{204}Pb$ for the alkali basalts from the Rhön. NHRL is the Northern Hemisphere Reference Line (Hart, 1984). Fields for mantle and crustal xenoliths and mafic alkaline lavas as in Fig. 6.

Figure 9: Measured O-isotope compositions (shown as $\delta^{18}O$ values relative to SMOW) vs. LOI for tephrites, phonolites and trachytes. Using the correction procedure outlined by Ferrara et al. (1985), LOI-corrected $\delta^{18}O$ values of between 5.5 and 7.2 ‰ for LOI=0.5 are calculated. Also shown are the corrected values of the alkali basalts from Freerck-Parpatt (1990) and Jung & Hoernes (2000) for comparison. These data have also been recalculated for a LOI value of 0.5% to allow for comparison with the data for the more differentiated rocks.

Figure 10: (a) Nb, (b) Zr, (c) Pb, (d) Rb and (e) Li vs. $^{143}Nd/^{144}Nd$ ratio for tephrites, phonolites and trachytes (this study) and alkali basalts from Jung and Hoernes (2000). Note that the distribution of the differentiated rocks follow two different paths. One path is characterized by constant

$^{143}Nd/^{144}Nd$ and increasing Nb, Zr, Pb, Rb and Li concentrations and is interpreted to result from fractional crystallization processes. The other path is consistent with an assimilation-fractional crystallization paths with decreasing $^{143}Nd/^{144}Nd$ and increasing Nb, Zr, Pb, Rb and Li concentrations. For the fractional crystallization (FC) calculations, model parameters are 84 ppm Nb, 250 ppm Zr, 5 ppm Pb, 40 ppm Rb, 10 ppm Li and $^{143}Nd/^{144}Nd$: 0.512800 (45 ppm Nd) for a hypothetical starting basanite. For the AFC calculation, model parameters are 74 ppm Nb, 237 ppm Zr, 5 ppm Pb, 34 ppm Rb, 10 ppm Li and $^{143}Nd/^{144}Nd$: 0.512824 (46 ppm Nd) for the starting basanite (sample 18 from Jung, 1995 and Jung and Hoernes, 2000) and 29 ppm Nb and $^{143}Nd/^{144}Nd$: 0.512608 (42.6 ppm Nd) for the lower crustal contaminant (sample S 1; Stosch and Lugmair, 1984). Nb concentration data are not available from granulite sample S 1 but were estimated using 2.02 ppm Ta from sample S 1 (Loock et al. 1990) and an inferred Nb/Ta ratio of 14.4 which is the average of 13 lower crustal xenoliths with subchondritic Nb/Ta ratios given by Mengel (1990). Lithium and Zr abundances for S 1 are not available and we chose 6 ppm Li and 130 ppm Zr for the lower crustal contaminant. These estimates are close to or within the range of lower crustal xenoliths from world-wide studies (Li: 3.3-11 ppm; Zr: 68-206 ppm; Rudnick and Gao, 2004) and from the CEVP (7-21 ppm Li, 93-164 ppm Zr; Mengel et al., 1990). Concentrations of Pb and Rb for S 1 are taken Rudnick and Goldstein (1990) and Stosch and Lugmair (1984). Bulk Kds for Nb, Zr, Pb, Rb and Li are 0.18, 0.19, 0.35, 0.12 and 0.18, resp. and were calculated using an estimated fractionating mineral assemblage (13.5 % olivine, 24 % clinopyroxene, 12.5 % amphibole, 24 % plagioclase, 6.75 % magnetite, 0.2 % ilmente and 1.2 % apatite) from Wedepohl et al. (1994). Distribution coefficients for Nb, Zr, Pb, Rb and Li were those from Adam et al. (1993) and Adam and Green (2006) for olivine, clinopyroxene and amphibole, Matsui et al. (1997), Ewart and Griffin (1994) and Villemant et al. (1981) for plagioclase, Ewart and Griffin (1994) and Zack and Brumm (1998) for magnetite/ilmenite and Mahood and Stimac (1993) for apatite. Model calculations indicate up to 60% assimilation of these hypothetical lower crustal rocks.

Figure 11: $^{143}Nd/^{144}Nd$ vs. $^{207}Pb/^{204}Pb$ for alkali basalts differentiated alkaline lavas from the Rhön. Lines show the results of AFC calculations according to DePaolo (1981). Model parameters are 51 ppm Nd, $^{143}Nd/^{144}Nd$ = 0.512851, 5 ppm Pb; $^{207}Pb/^{204}Pb$: 15.60 for the parental basanite (sample 1a from Jung and Hoernes, 2000 and Jung et al. 2005) and 42.6 ppm Nd, $^{143}Nd/^{144}Nd$: 0.512608, 5.1

ppm Pb, $^{207}Pb/^{204}Pb$: 15.66 for the hypothetical lower crustal rock (sample S 1 from Rudnick and Goldstein, 1990). Bulk Kds for Nd and Pb were 0.5 and 1.0, respectively. r (the ratio of mass assimilated to mass fractionated) was set at 0.4.

Table 1. Sample locations of differentiated alkaline rocks from the Rhön area

Sample no.	Rock type	Map No	Map name	Locality	Latitude (N)	Longitude (E)
11.F	Tephrite	5325	Spahl	Suchenberg	50°39'56128	09°50'35640
11.G	Tephrite	5325	Spahl	Suchenberg	50°39'56128	09°50'35632
8	Tephrite	5225	Geisa	Dachsberg	50°42'56227	09°50'35628
14	Tephrite	5424	Fulda	Farrod	50°35'56073	09°50'35588
27	Tephrite	5525	Gersfeld	Steinwand	50°29'55955	09°40'35613
28	Tephrite	5525	Gersfeld	Steinwand	50°29'55955	09°50'35613
29	Tephrite	5525	Gersfeld	Steinwand	50°29'55955	09°50'35613
9	Ph.Tephrite	5225	Geisa	Kirchberg	50°42'56219	09°50'35645
13	Ph.Tephrite	5325	Spahl	Seelesberg	50°39'76102	09°50'35685
26	Teph. Phon.	5525	Gersfeld	Steinwand	50°29'55955	09°50'35613
15	Phonolite	5425	Kleinsassen	Hohlstein	50°30'56038	09°50'35637
3	Phonolite	5425	Kleinsassen	Kesselberg	50°30'56024	09°50'35668
16	Trachyte	5425	Kleinsassen	Sternkuppel	50°30'56997	09°50'35640
17	Trachyte	5424	Fulda	Alschberg	50°30'55991	09°45'35577

-Table 2: Major and trace element composition of tephrites (T), tephritic phonolites (TP), phonolitic tephrites (PT), phonolites (P) and trachytes (Tr) from the Rhön area. LOI: Loss on ignition. Standard values for JB 3 are from Govindaraju (1984) and REE values for an in-house standard (alkaline basalt BB) are from Engelhardt (1990) calibrated against several international rock standards.

Sample No.	11.F	11.G	8	14	27	28	29	9	13	26	15	3	16	17	JB3 (rec.)	JB 3
Rock type	T	T	T	T	T	T	T	PT	PT	TP	P	P	Tr	Tr		
SiO_2	45.90	44.50	46.52	43.91	45.80	45.60	46.70	51.24	51.38	55.40	60.94	59.80	58.88	59.41	51.03	51.04
TiO_2	2.62	2.89	2.43	2.75	2.40	2.40	2.60	1.80	1.61	0.80	0.47	0.24	0.71	0.63	1.43	1.45
Al_2O_3	15.65	14.53	16.83	14.73	16.20	15.90	15.90	17.94	17.91	19.70	18.83	19.68	19.62	18.56	17.37	16.89
Fe_2O_3	5.68	6.78	4.79	5.69	5.40	5.20	5.20	3.71	3.43	2.40	2.19	1.89	3.02	2.67	11.93	11.88
FeO	4.91	5.53	5.36	6.42	5.30	5.80	5.90	3.98	3.70	1.60	0.59	0.45	0.73	0.75	n.d.	n.d.
MnO	0.26	0.23	0.25	0.23	0.20	0.30	0.20	0.30	0.30	0.30	0.24	0.36	0.22	0.29	0.18	0.16
MgO	3.92	5.22	3.31	4.82	4.70	4.90	4.90	2.32	2.10	0.90	0.46	0.20	0.68	1.08	5.16	5.20
CaO	9.87	9.90	8.78	9.93	8.80	9.60	8.90	6.94	6.26	4.50	1.75	1.16	2.94	1.86	9.77	9.86
Na_2O	4.31	3.67	4.36	3.26	3.90	3.10	2.90	5.45	5.18	5.30	6.71	7.78	5.86	5.43	2.77	2.82
K_2O	2.49	1.53	2.69	2.50	2.60	2.30	2.10	2.90	3.31	4.70	5.72	5.48	4.52	5.59	0.76	0.78
P_2O_5	1.48	1.28	1.74	1.64	1.10	1.20	1.30	0.76	0.76	0.10	0.02	0.04	0.20	0.12	0.28	0.29
LOI	1.99	3.10	2.41	3.13	3.10	3.10	2.60	1.98	4.19	3.80	1.45	3.11	2.85	3.14	n.d.	n.d.
Sum	99.08	99.16	99.47	99.01	99.50	99.40	99.20	99.32	100.1	99.50	99.37	100.2	100.2	99.53	100.71	100.37
Li	19	14	14	13	22	15	16	18	21	25	25	30	13	33		
Rb	68	38	59	69	73	58	58	84	72	127	148	149	131	179	16	13
Zn	173	157	163	160	147	141	148	183	159	162	175	180	163	197	109	106
Co	27	37	16	33	28	28	28	9	15	3	2	2	2	2	36	36.3
Cu	13	21	3	18	13	24	24	3	6	3	3	3	3	3	151	198
Ni	3	10	3	8	31	29	29	3	3	3	3	3	3	3	33	38.8
Pb	13	8	6	8	8	7	6	12	11	15	13	9	9	23	5	5.5
Sr	1422	1272	2158	1841	1931	1977	1716	2025	2232	1622	94	247	631	1914	411	395
V	211	255	117	223	181	187	154	71	96	42	8	5	13	24	367	383
Ba	1081	979	1122	978	1262	1175	1041	1271	1842	2131	366	237	1861	1372	226	251
Y	49	40	50	48	40	38	34	45	47	42	33	46	43	61	25	27
Cr	6	10	3	13	31	30	27	4	3	3	3	3	3	3	58	60.4
Zr	594	485	448	496	410	371	385	681	537	746	1002	1104	720	773	93	98.3
Nb	150	125	112	130	101	92	140	166	136	157	184	235	186	262	5	2.3
Sc	12	13	6	12	8	12	13	4	4	1	1	1	1	1	32	33.3
															BB (rec.)	BB
La	117	99	108	99	89	87	54	140	105	140	140	127	150	166	48.0	47.2
Ce	226	189	224	200	167	185	104	265	212	245	240	233	279	327	92.0	91.0
Nd	94	79	93	93	71	78	49	106	89	73	55	82	103	98	43.0	42.4
Sm	18.10	15.20	18.60	15.20	14.10	12.30	7.50	15.60	15.20	13.00	8.10	15.30	14.00	10,1	8.4	8.1
Eu	5.33	3.92	5.58	3.51	3.77	3.07	2.31	5.10	4.09	3.21	1.81	2.88	3.80	3.11	2.5	2.5
Gd	15.50	12.40	13.80	10.70	9.50	9.20	7.10	11.40	13.20	7.80	6.60	10.70	13.00	9.30	6.8	6.9
Dy	10.40	8.10	9.90	7.00	6.00	5.70	4.90	9.80	7.10	4.60	5.60	8.20	10.00	7.50	4.7	4.5
Er	4.50	3.60	3.50	3.30	2.10	2.30	1.90	3.90	3.60	3.10	3.70	4.50	3.60	4.40	2.1	2.2
Yb	3.90	2.90	2.30	2.00	1.90	1.80	1.60	2.50	2.30	2.60	4.20	4.80	2.40	4.10	1.7	1.8
Lu	0.46	0.40	0.29	0.30	0.27	0.31	0.23	0.33	0.33	0.40	0.51	0.54	0.30	0.50	0.23	0.22

Table 3: Initial Sr, Nd, Pb and O isotope (in ‰ relative to SMOW) composition of tephrites, phonolites and trachytes from the Rhön area. Errors are 2 s (mean) in the last two digits. Pb isotopes were recalculated using U/Pb = 0.15 and Th/U = 4 for tephrites and U/Pb = 0.54 and Th/U = 3.3 for phonolites (Wedepohl et al. 1994). All initial ratios were recalculated using an age of 23 Ma which is within the range of 27-21 Ma for the age of volcanism quoted by Wedepohl et al. (1994). (m): measured, (i): initial, (l): leachate, (u): unleached, (r): residue; (corr.): corrected. n.d.: not determined. Initial $^{87}Sr/^{86}Sr$ ratios were recalculated using measured $^{87}Rb/^{86}Sr$ ratios and $^{87}Sr/^{86}Sr$ ratios obtained on the residue. Rb and Sr concentrations were measured by isotope dilution on the residues after leaching. Neodymium isotopes were corrected for $^{143}Nd/^{144}Nd$=0.512850 for the LaJolla standard and Sr isotopes were corrected for $^{87}Sr/^{86}Sr$=0.710240 for NBS987.

Sample	8	14	9	13	26	3	15	16	17
Rock type	Tephrite	Tephrite	ph. Theprite	Tephrite	teph. Phonolite	Phonolite	Phonolite	Trachyte	Trachyte
Laboratory	U Münster	MPI Mainz	MPI Mainz	U Münster	U Münster	U Münster	U Münster	MPI Mainz	MPI Mainz
$^{143}Nd/^{144}Nd$ (m)	0.512804	0.512787	0.512776	0.512775	0.512808	0.512816	0.512812	0.512770	0.512799
error	0.000004	0.000012	0.000013	0.000002	0.000004	0.000004	0.000002	0.000013	0.000013
Sm (ppm)	19.6	20.2	19.6	18.2	13.0	15.3	10.1	20.0	20.2
Nd (ppm)	83.0	93.0	101	82.0	73.0	82.0	55.0	103	98.0
$^{147}Sm/^{144}Nd$	0.138	0.143	0.127	0.146	0.117	0.123	0.121	0.128	0.135
$^{143}Nd/^{144}Nd$ (i)	0.512784	0.512771	0.512761	0.512758	0.512794	0.512798	0.512797	0.512757	0.512798
$^{87}Sr/^{86}Sr$ (l)	0.704143	0.704336	0.704322	0.704241	0.704255	0.710446	0.705140	0.705141	0.703875
error	0.000011	0.000011	0.000014	0.000010	0.000012	0.000011	0.000015	0.000012	0.000013
$^{87}Sr/^{86}Sr$ (u)	0.703866	0.703980	0.703968	0.704011	0.703827	0.706972	0.705081	0.704548	0.703757
error	0.000010	0.000014	0.000012	0.000011	0.000014	0.000012	0.000014	0.000013	0.000011
$^{87}Sr/^{86}Sr$ (r)	0.703879	0.703669	0.703620	0.703773	0.703711	0.704502	0.704864	0.704001	0.703729
error	0.000009	0.000012	0.000013	0.000007	0.000012	0.000007	0.000012	0.000012	0.000013
Rb (ppm)	59	69	84	72	127	149	148	131	179
Sr (ppm)	2158	1842	2025	2238	1629	247	94	631	1914
$^{87}Rb/^{86}Sr$	0.076	0.103	0.115	0.089	0.215	1.666	4.349	0.573	0.258
$^{87}Sr/^{86}Sr$(i)	0.703854	0.703635	0.703583	0.703744	0.703641	0.703958	0.703443	0.703814	0.703645
$\delta^{18}O$ (m)	7.4	8.7	7.9	8.1	8.9	8.9	7.2	8.4	9.2
LOI (%)	2.41	3.13	1.98	3.19	3.80	3.11	1.45	2.85	3.14
$\delta^{18}O$ (corr.)	6.0	6.7	6.8	5.4	6.4	7.0	6.4	6.2	7.2
$^{206}Pb/^{204}Pb$ (i)	19.099	19.313	n.d.	19.086	19.077	19.130	19.104	19.098	19.072
error	0.001	0.001	n.d.	0.002	0.001	0.001	0.001	0.002	0.001
$^{207}Pb/^{204}Pb$ (i)	15.619	15.630	n.d.	15.621	15.621	15.627	15.618	15.622	15.625
error	0.001	0.001	n.d.	0.001	0.001	0.001	0.002	0.002	0.001
$^{208}Pb/^{204}Pb$ (i)	38.937	39.135	n.d.	38.927	38.928	38.967	38.925	38.915	38.903
error	0.003	0.003	n.d.	0.004	0.004	0.002	0.005	0.005	0.003

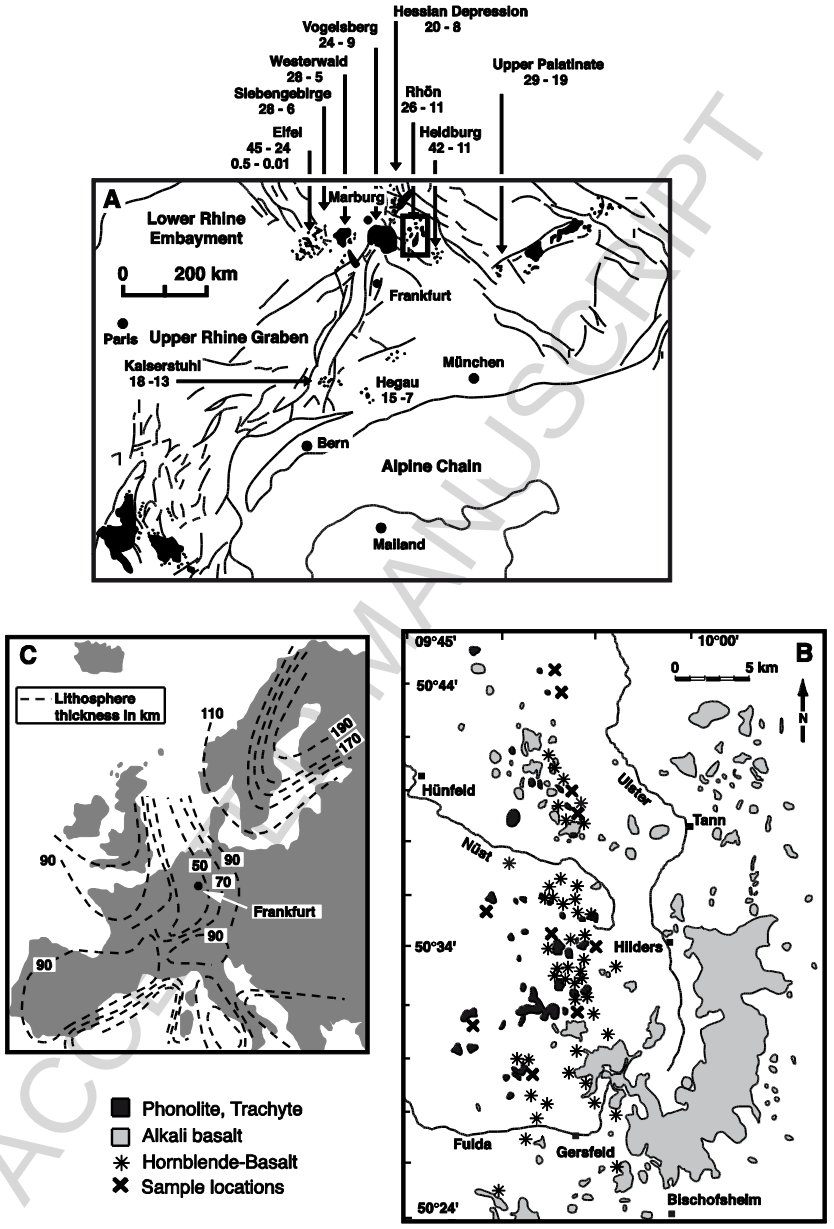

Fig. 1

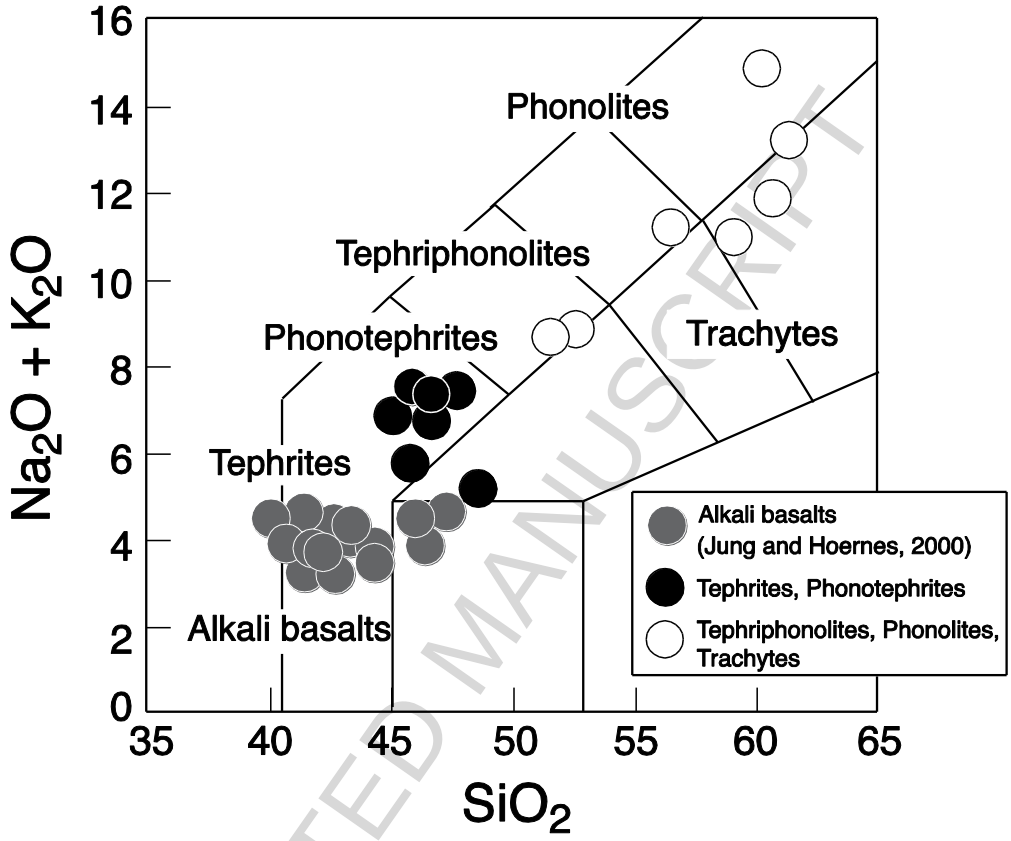

Fig.2

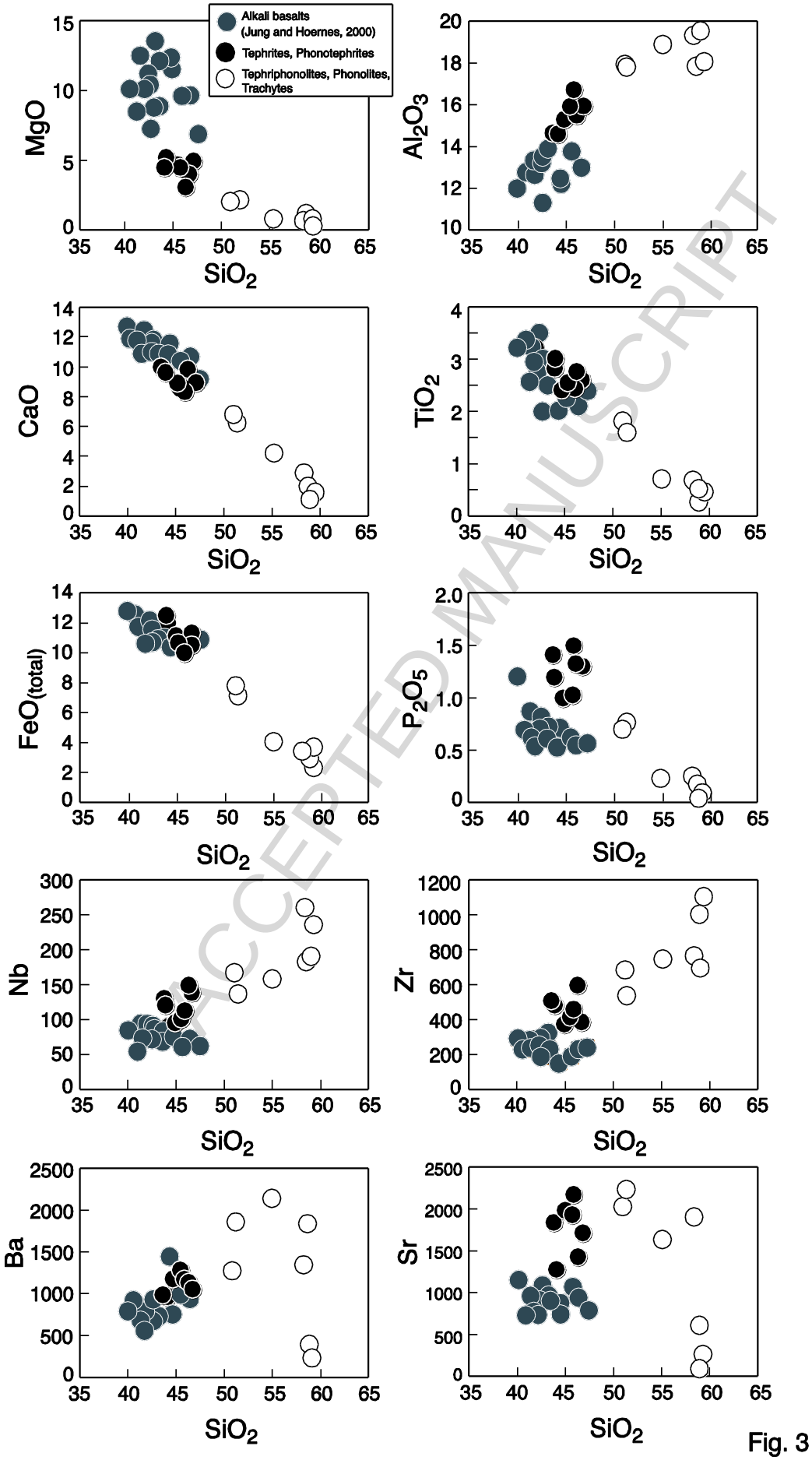

Fig. 3

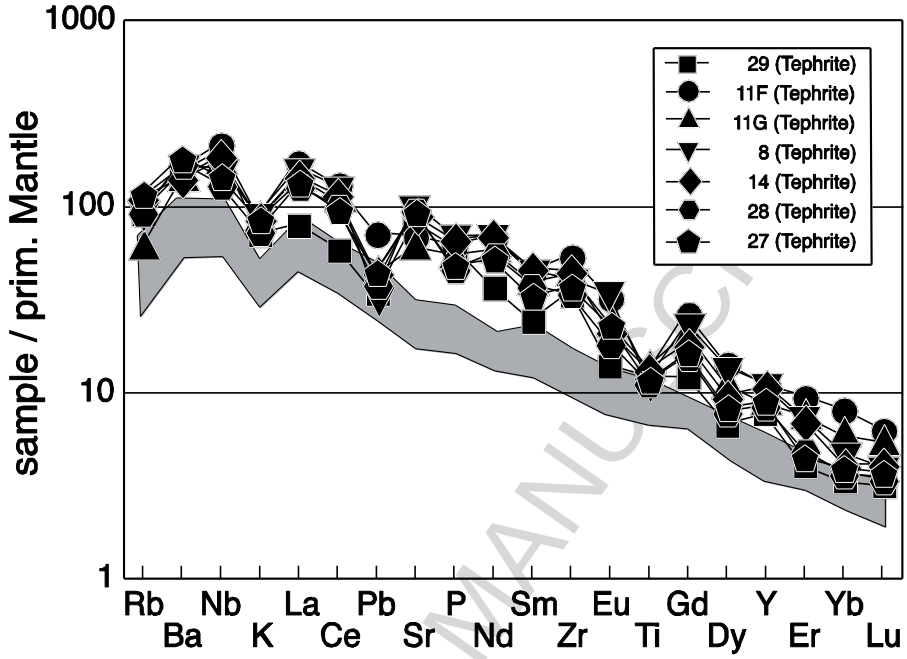

Fig. 4a

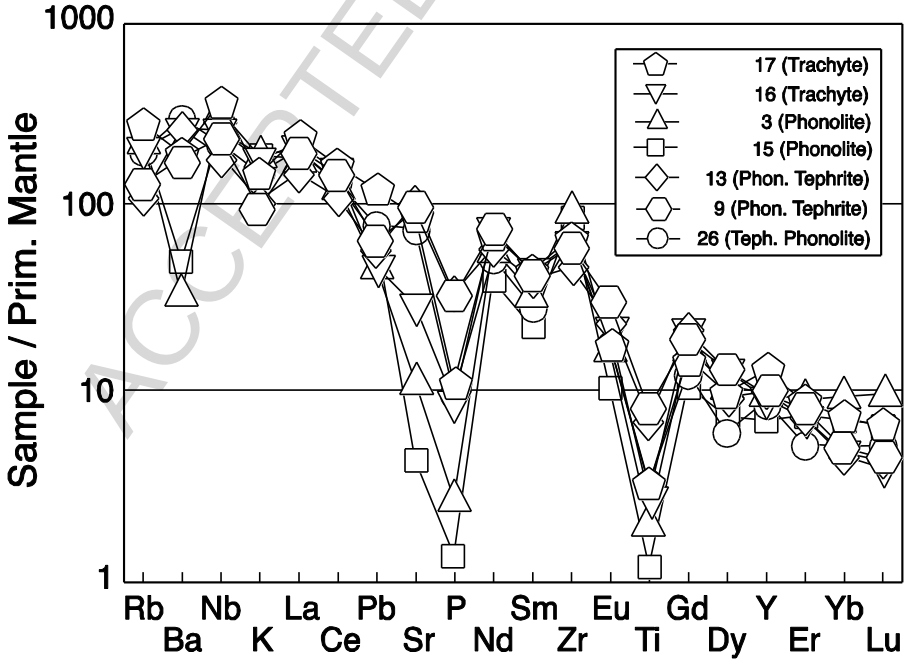

Fig. 4b

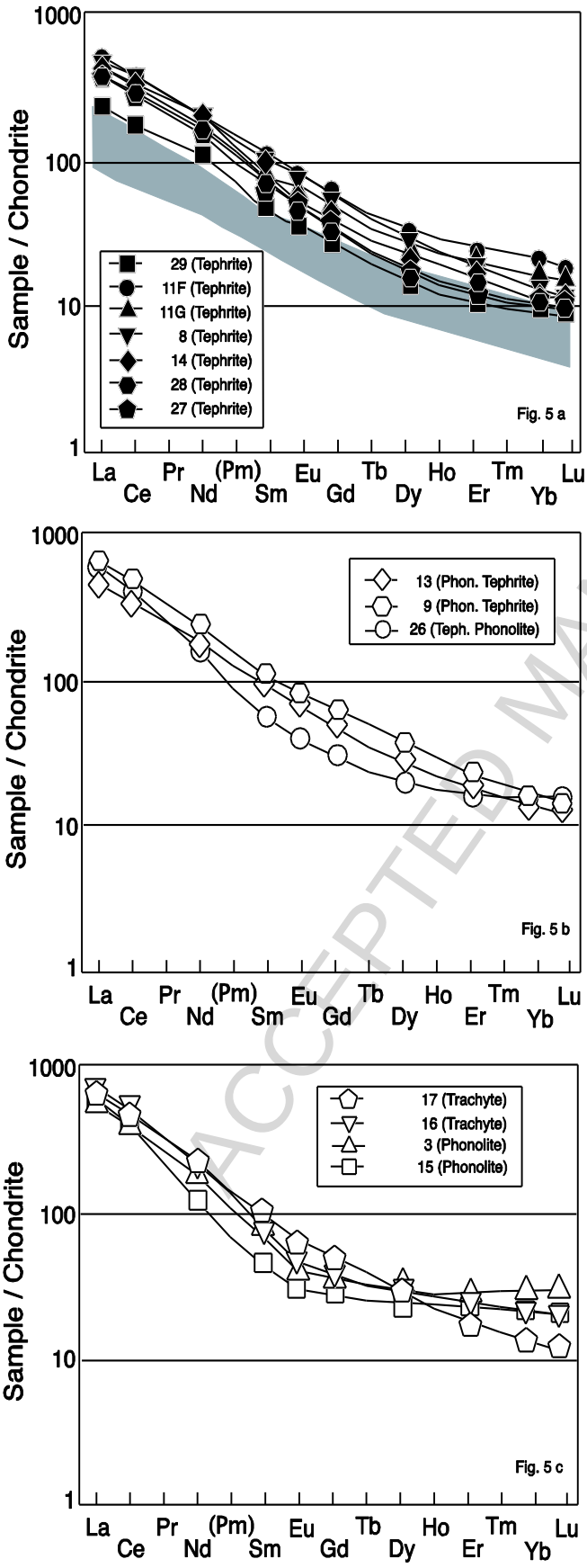

Fig 5

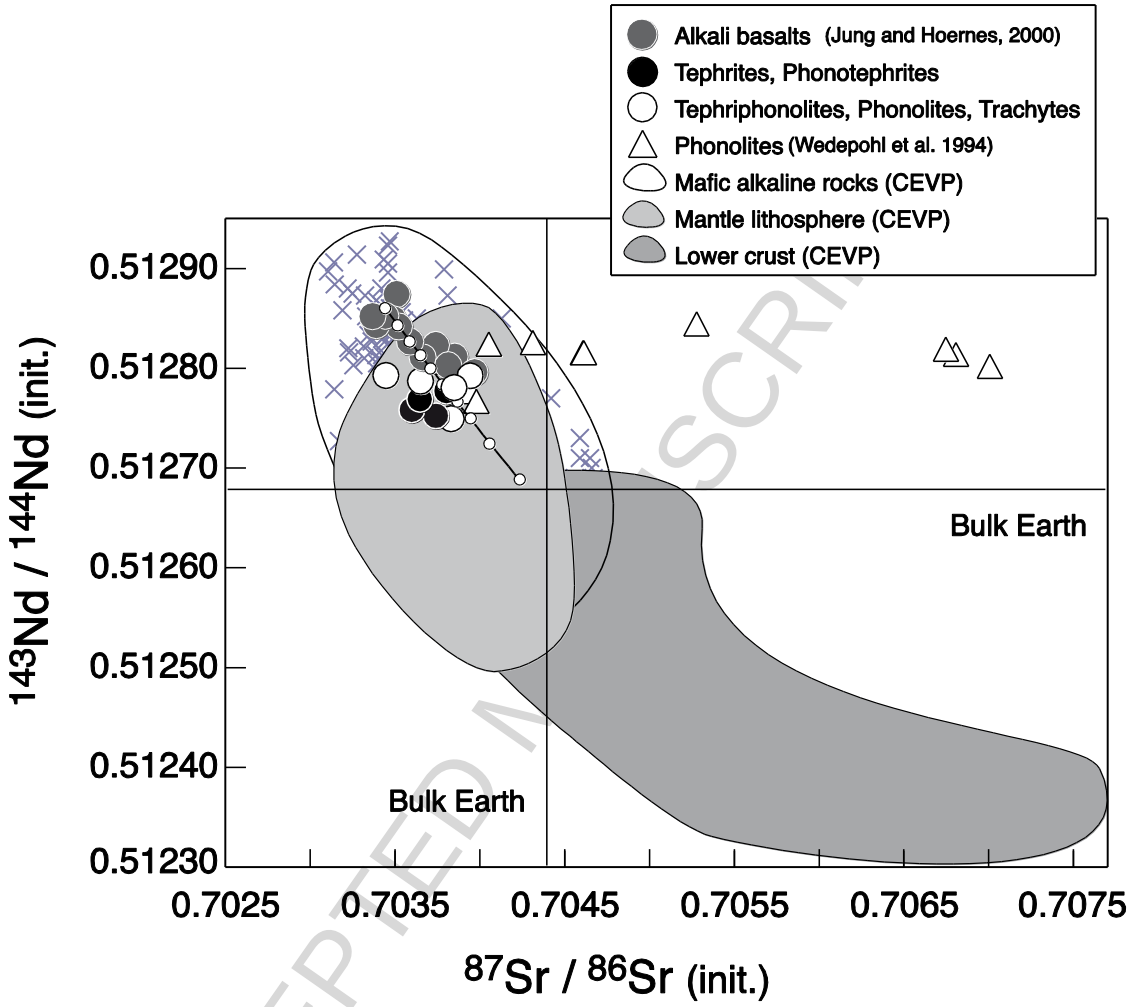

Fig. 6

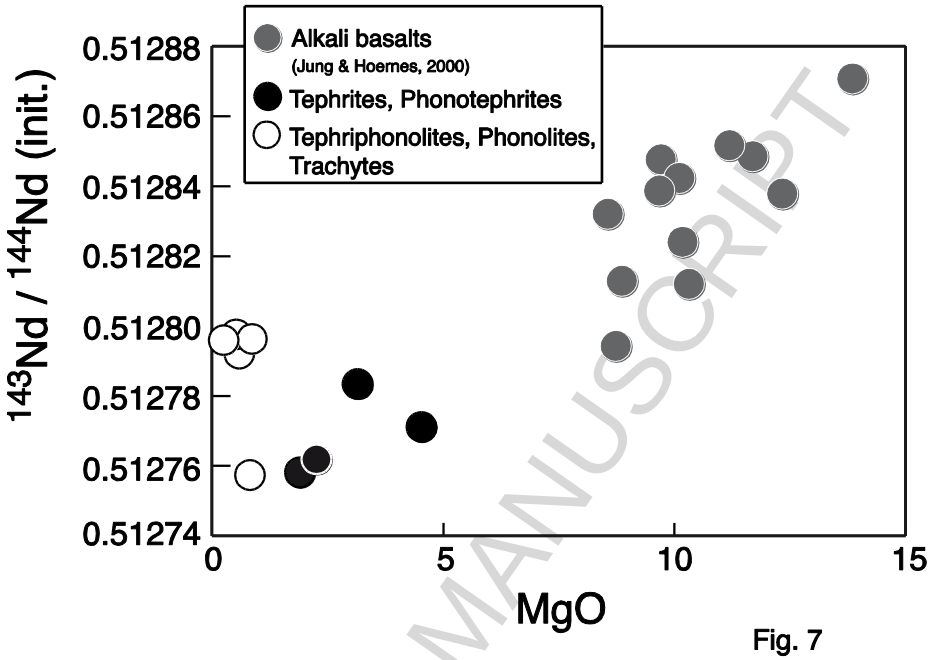

Fig. 7

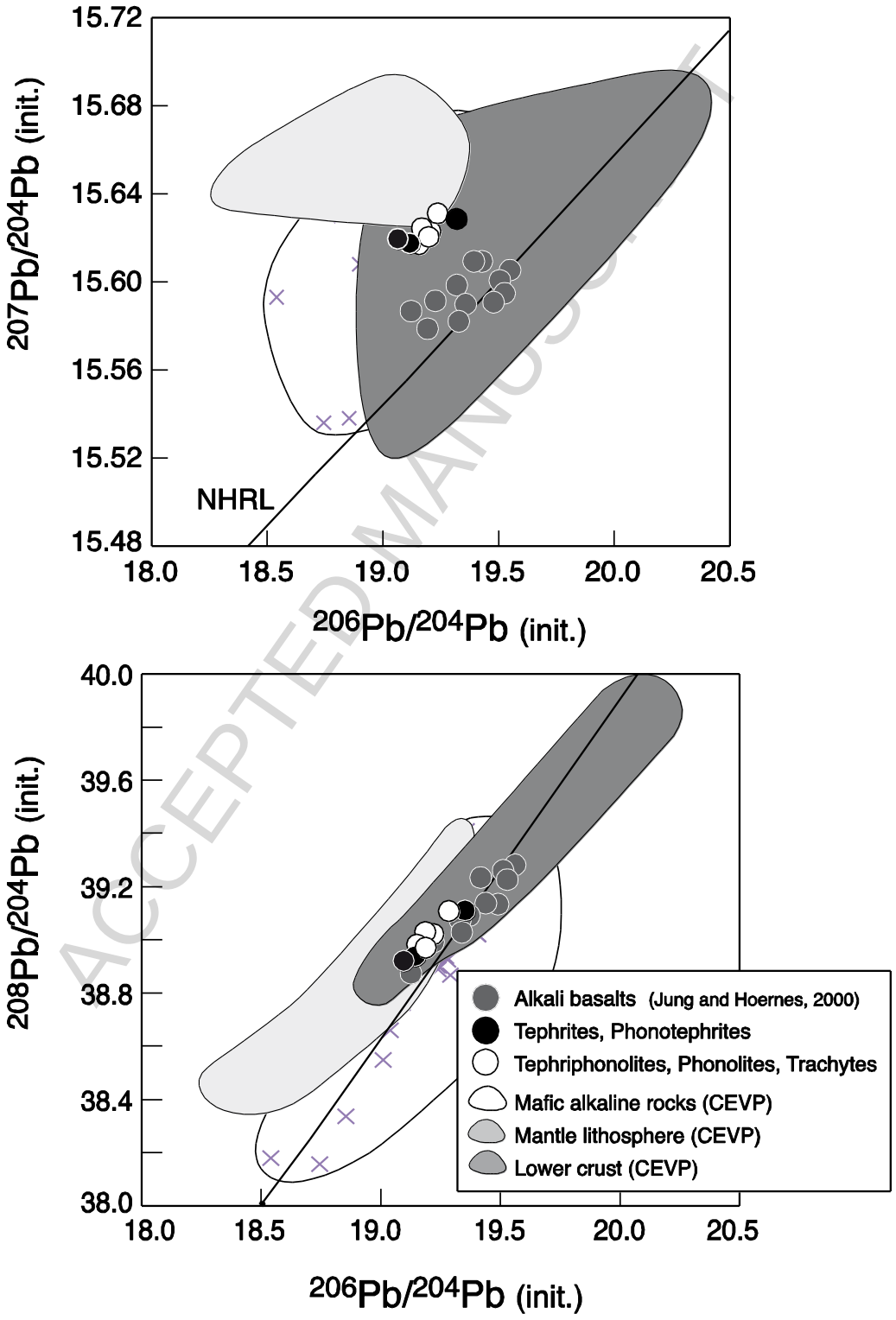

Fig. 8

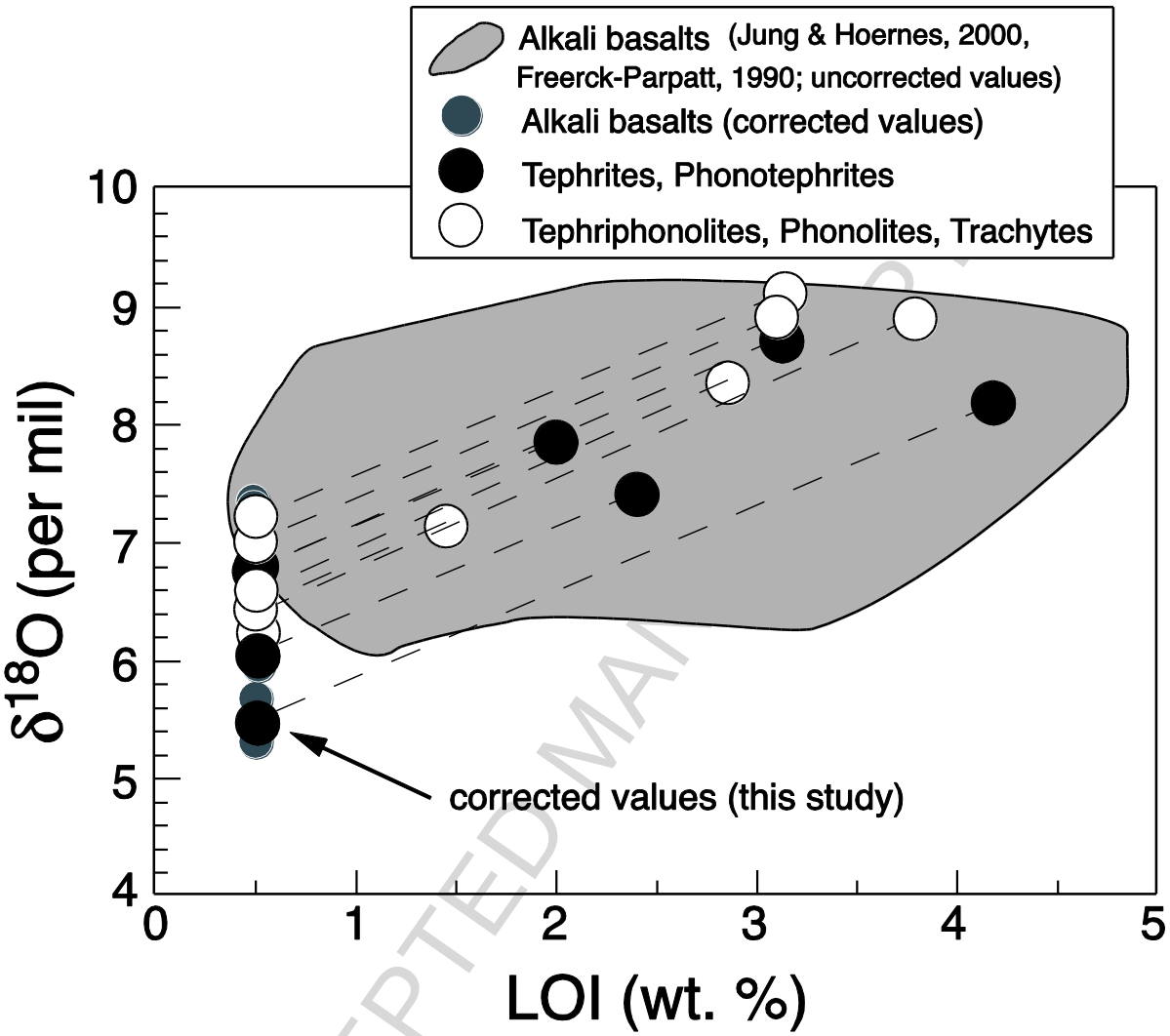

Fig. 9

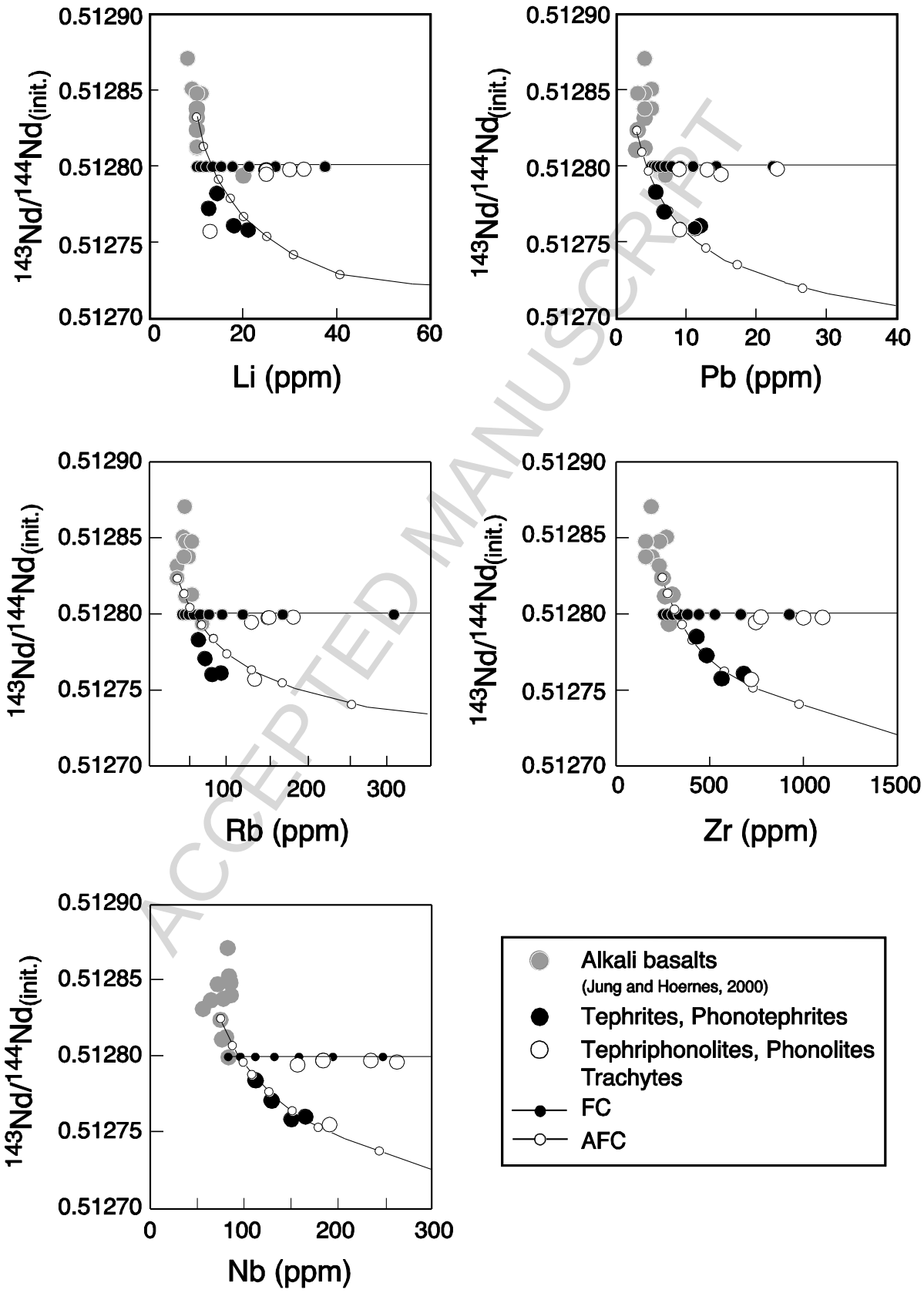

Fig 10

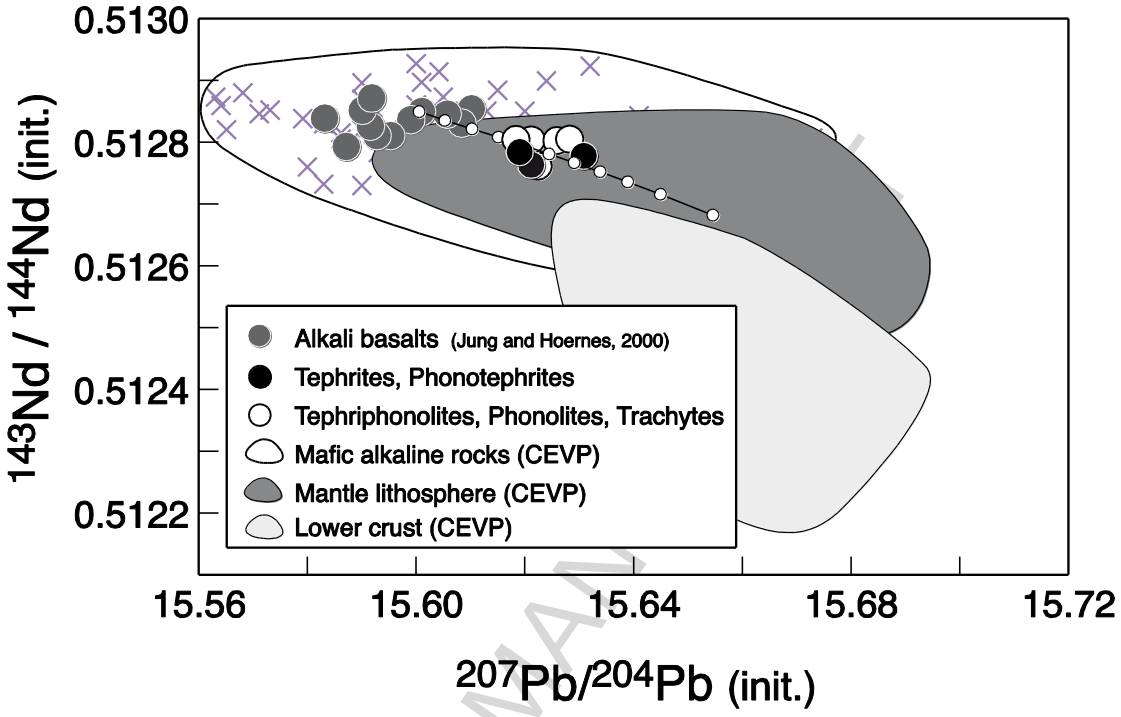

Fig. 11

Highlights

Some differentiated alkaline rocks may evolve by FC or AFC but not both

Analyses of acid-leached samples necessary to detect unsupported ^{87}Sr

Crustal contamination hardly detectable in high-Sr lavas but obvious in low-Sr lavas

Deep crustal contamination confirmed by high-precision Pb double-spike data

Positively correlated $^{87}Sr/^{86}Sr$ ratios - $\delta^{18}O$ values also indicate crustal contamination